Covalent grafting of alkyl chains on laser-treated titanium surfaces through silanization and phosphonation reactions

Iryna Tomashchuk, Liudmyla Kostenko, Jean-Marie Jouvard, Luc Lavisse, María del Carmen Marco de Lucas

Covalent grafting of alkyl chains on laser-treated titanium surfaces through silanization and phosphonation reactions

Iryna TOMASHCHUK[a*], Liudmyla KOSTENKO[b], Jean-Marie JOUVARD[a], Luc LAVISSE[c], María del Carmen MARCO de LUCAS[c]

[a] Laboratoire Interdisciplinaire Carnot de Bourgogne, UMR 6303 CNRS, Université Bourgogne Franche-Comté, 12 rue de la Fonderie, 71200 Le Creusot, France. E-mails: iryna.tomashchuk@u-bourgogne.fr; jean-marie.jouvard@u-bourgogne.fr.

[b] Faculty of Chemistry, Taras Shevchenko National University of Kyiv, Lva Tolstoho Street 12, 01033 Kyiv, Ukraine; E-mail: lskostenko69@gmail.com .

[c] Laboratoire Interdisciplinaire Carnot de Bourgogne, UMR 6303 CNRS, Université Bourgogne-Franche Comté, 9 Avenue A. Savary, BP 47 870, F-21078 Dijon Cedex, France. E-mails: luc.lavisse@u-bourgogne.fr; delucas@u-bourgogne.fr.

*corresponding author

Abstract

This work evaluates the efficiency of silanization and phosphonation reactions for the grafting of alkyl chains on the surface of titanium treated by nanosecond laser. The light blue squama-like oxide layers with dominating anatase and rutile were obtained. The silanization using alkoxysilanes with C_{12} and C_{18} alkyl chains was attempted in tetrahydrofuran, in pure liquid phase and in vapor phase. The phosphonation with octylphosphonic acid was performed in boiling water solutions. The obtained surfaces were characterized by Raman and X-ray photoelectron spectrometry, scanning electron microscopy and energy dispersive X-ray spectroscopy. Their hydrophobicity was evaluated using static contact angle measurements.

The modification in pure liquid silane and in vapor phase allowed obtaining high loadings (6 and 10 at.% Si respectively) of grafted groups and the formation of polycondensed silane layers. The silanization in tetrahydrofuran resulted in partial monolayer coverage. The phosphonation in boiling water solutions allowed obtaining significant P loading (up to 7 at.%) and full monolayer coverage. Both

silanization and phosphonation increased the hydrophobicity of laser-treated surfaces. However, the modification with octylphosphonic acid in water solutions is more appropriate since milder conditions of chemical functionalization and lower concentrations of the modifier are necessary to obtain similar organic loading and hydrophobicity.

Keywords: laser surface treatment, titanium oxides, silanization, phosphonation

1. Introduction

The covalent grafting of organic molecules to the surface of titanium oxide films opens interesting perspectives for the creation of novel materials for electronics, solar cells, sensors, biomaterials, self-cleaning surfaces, surface-tension-controlled microfluidic devices, implants with enhanced biocompatibility [1,2], photocatalytic supports [3] and so on. The existence of a stable native oxide film on the surface of titanium and its alloys allows the direct chemical functionalization of the metallic surface. Dahany et al. [4] characterized the self-assembled monolayers (SAM) of various diphosphonic acids as a stable interface system for the immobilization of biological molecules on the surface of titanium. Adden et al. [5] described the multi-step binding of amine-containing molecules on titanium surfaces for enhanced biocompatibility. Viornery at al. [6] demonstrated the increase of calcium phosphate deposition on the surface of titanium functionalized with tri- and tetra- phosphonic acids, which improves adhesion between bone and titanium-based implants. For the prevention of implant-associated infections, Vaithilingam et al. [7,8] performed bonding of drug molecules to phosphonic SAM layers formed on titanium parts fabricated by selective laser melting.

As the bonding of organic molecules to the native oxide layer happens mainly through the interaction with Ti-OH groups, the formation of more developed oxide layer allows increasing the organic loading during the chemical functionalization. Micrometric oxide films can be created on the surface of titanium and its alloys by thermochemical or wet oxidation, electrochemical deposition, laser materials processing, physical vapor deposition etc. The nanosecond laser treatment of titanium surfaces allows creation of well-developed oxide layers having complex micrometric patterning [9,10,11,12] that cannot be obtained by common electrochemical and thermal oxidation methods. High precision energy

supply associated with flexibility of scanning paths, pulse frequency, beam energy etc. allows producing localized oxide layers of various nature, thickness and morphology [13,14, 15]. The controllable and reproducible roughness of such oxide surfaces can from one hand tune the wetting properties through the formation of air micro-pockets in the micrometric grooves, and from another hand promote polymer adhesion of due to the enhanced mechanical interlocking during the fusion joining processes [16,17]. The use of laser processing is also time-saving compared to the classical oxidation in the furnace and induces very local heating of the product.

In case of maximum oxygen insertion, associated with high fluence of laser radiation, titanium oxide films have a stratified structure composed by superficial Ti(IV) and Ti(III) oxide nanoparticles and by compact layers, where stoichiometric Ti(IV) and Ti(III) oxides are progressively replaced by sub-stoichiometric oxides and oxynitrides [14, 18,19].

The covalent immobilization of organic molecules on metallic and oxide surfaces is a flourishing field of modern surface chemistry. Two main groups of chemical modifiers were successfully applied for the functionalization of TiO_2 powders and films: organosilanes and phosphonic derivatives. Both allow attaining the similar density of grafted groups (4-5 groups/nm² [2, 20]), however, phosphonic derivatives usually show higher affinity to titanium oxide compared to silanes [2] and form Ti-O-P bonds that are more stable to hydrolysis over a wide pH range compared to Si-O-Ti bonds [20]. Another important difference between these two groups of modifiers consists in the exclusive formation of heterocondensed (Ti-O-P) bonds leading to the creation of self-assembled monolayers for the phosphonic derivatives, whereas during the immobilization of silanes, the heterocondensation with the surface (Si-O-Ti) concurrences with homocondensation (Si-O-Si) associated with the formation of thick polycondensed layers, especially in presence of water [20]. Along with standard silanization procedures in organic solvents [1,2,21], the creation of silane layers can be also performed in vapor phase [22], whereas the phosphonation is usually performed in water solutions [3]. Both kinds of modifiers have a wide range of commercially available products with different functional groups.

The organic layers covalently bonded to the laser-oxidized titanium surface can enhance the adhesion in titanium/polymer joints currently finding many novel applications in microelectronics [23], microfluidics [24], aerospace [25] and automotive lightweight design [26,27] and so on. As polymers

and metals have very different physical properties, their bonding is usually based on the mechanical interlocking, when a melted polymer solidifies in the micrometric pattern previously created on the metallic surface [16]. The nature of the chemical interaction between a melted polymer and titanium surface has little studied. Kondoh et al. have reported XPS analysis showing the formation of Ti-C and Ti-F bonds in laser assembly of poly(vinylidene fluoride) [23] and Teflon [24] with titanium for microelectromechanical systems, and a high-temperature assembly of polyamide66 with titanium where the presence of C=O bonds at the metal/polymer interface was related to improved bond strength [27]. Tan et al. [28] recently demonstrated the positive effect of a grafted aminosilane layer on the adhesion of carbon fiber reinforced polyether-ether-ketone (PEEK) to the titanium surface oxidized by micro-arc, due to the formation of hydrogen bonds between the aminogroups and the polymer chains.

The covalent chemical modification of the titanium surface oxidized and patterned by laser processing would create a resilient hybrid organic-inorganic interface, where the chemical affinity to the polymer can be controlled by the choice of tailored groups. To obtain the maximal effect on the polymer adherence, such hybrid interface should have uniform and maximal possible loading of grafted groups. Some recent studies [10,11] report the silanization of laser-processed titanium surfaces by dipping in diluted (~ 1 mM) organic solutions followed by drying at high temperature. However, no studies on the phosphonation of laser-treated titanium surfaces are available.

The aim of the present work is to produce covalently grafted organic layers with maximum modifier loading on the surface of titanium treated by nanosecond laser, in view of future development of robust solutions enhancing the adhesion strength during bonding with polymers. The efficiency of silanization and phosphonation reactions was evaluated. The silanization using alkoxysilanes with C_{12} and C_{18} alkyl chains was attempted in boiling tetrahydrofuran (THF) solution, in pure liquid phase and in vapor phase, whereas phosphonation with octylphosphonic acid was performed in boiling water solutions. The modified surfaces were characterized by Raman spectroscopy, X-ray photoelectron spectrometry (XPS) and scanning electron microscopy (SEM) coupled with energy dispersive X-ray spectroscopy (EDS). The hydrophobicity of the surfaces was evaluated using static contact angle measurements.

2. Materials and methods

2.1. Materials and chemicals

1 mm thick Grade 1 ASTM B265 titanium plates by GoodFellow cut into 1 cm x 1 cm squares were used as substrates. Technical grade dodecyltriethoxysilane (DDTES) and octadecyltrimethoxysilane (ODTMS) by Sigma Aldrich were used in the silanization experiments. A 97% pure octylphosphonic acid (OPA) by Sigma Aldrich was used for phosphonation experiments. A 99.8% pure tetrahydrofuran (THF) by Honeywell and distilled water were used as solvents.

2.2. Surface laser treatment

Titanium samples previously polished down to 600-grit with SiC paper were treated in ambient atmosphere using a double frequency pulsed neodymium-doped yttrium aluminum garnet (Nd:YAG) laser Kaluti System (λ=532 nm) with Gaussian energy distribution, spot diameter of 60 µm and pulse time of 5 ns. On the basis of previous work [29], the average beam power was fixed to 1.7 W, pulse frequency to 10 kHz and scanning speed to 12 mm/s. Linear scan lines applied in back-and-forth directions were spaced by 10 µm and formed a total surface of 1 cm². In the preliminary experiments, spacings of 20 and 50 µm were also tested, however, they demonstrated lower oxygen insertion and silane loading (using Si-V modification scheme, see section *2.3*).

Prior to chemical modification, in order to remove free or weakly-adhered oxide particles, the plates underwent 10 min ultrasound cleaning (US) in ethanol followed by 30 min drying at 90°C.

2.3. Chemical functionalization

The silanization was attempted through three different approaches:

- samples Si-V were suspended above the pure boiling ODTMS (T_{boil} = 170°C) in a 50 ml single-neck flask equipped with a reflux condenser and contacted the silane vapors for 6 h;
- samples Si-D were covered with a droplet of pure DDTES (T_{boil} = 234°C) and heated to 90° for 2.5 h in ambient atmosphere;
- samples Si-S were immerged in a 5.6 mM solution of DDTES in THF (T_{boil} = 66°C) in a 50 ml single-neck flask equipped with a reflux condenser and boiled for 6 h.

The phosphonation with OPA was performed in a 50 ml single-neck flask equipped with a reflux condenser, in boiling water solutions with increasing OPA concentration for the duration of 6 h: 5.6 mM (sample P5.6), 10 mM (sample P10), 16.8 mM (sample P16.8), 50 mM (sample P50) and 100 mM (sample P100).

After chemical functionalization, all samples were washed with ethanol and dried for 30 min in ambient atmosphere at 90°C.

2.3. Characterization methods

Topography observations and elemental analysis were performed using a scanning electronic microscope JSM-6610LA (Jeol), equipped with an EDS analyzer operating at 20 kV.

XPS measurements with a Kα1 Al source (1486.7 eV) were performed with PHI 5000 VersaProbe (ULVAC-PHI, Inc) at 10^{-7} Pa, a 200 µm wide analysis spot, a takeoff angle of 45° and pass energy of 187 eV/58.7 eV for survey spectra and high-resolution spectra respectively. XPS measurements with a novel hard X-ray source Kα1 Cr (5414.9 eV) suitable for the analysis of buried surfaces were performed with Phi Quantes Scanning Dual X-ray Photoelectron Microprobe (ULVAC-PHI, Inc) at 10^{-7} Pa, a 100 µm wide analysis spot, a takeoff angle of 45° and pass energy of 280 eV/55 eV for survey spectra and high-resolution spectra respectively. In both cases, the energy steps of 0.1 eV and 0.05 eV were used for survey spectra and high-resolution spectra respectively. The binding energies were referred to C-C & C-H position set at 285.0 eV. The processing of the spectra was performed with Multipak and Casa XPS software. The attribution of the components in high-resolution spectra was made using XPS database [30] and existing literature cited in the discussion.

The samples were analyzed by microRaman spectroscopy at room temperature using a Renishaw in Via spectrometer in backscattering configuration. The spectra were recorded using a 532 nm wavelength laser as excitation source, the laser power was below 3 mW to avoid heating the samples and laser spot about 2 µm in diameter.

Contact angle measurements were repeated four times in static condition at ambient temperature using 6.32 µl droplet of deionized water deposited on the surface with a micro syringe.

3. Results and discussion

3.1. Characterization of laser-treated titanium surfaces

For the chosen operational parameters, a standalone line of laser pulses on titanium surface (Figure 1a) was composed by slightly elliptic melted zones having the length of 89 µm and width of 73 µm, with the oxide particles expulsed at the borders of the crater. The used linear speed resulted in a 61% overlap in the direction of the scan. During the surface treatment, the scan direction was inversed for each new line (red arrows on the right of Figure 1b), with the offset between the lines of 10 µm, resulting in a 86% overlap in the direction perpendicular to the scan line. The produced squama-like topography (Figure 1b) was composed by the elevations formed by oxide particles at the borders of the impacts and the depressions corresponding to the overlapped melted zones.

The laser treatment conditions were chosen in order to create a structured surface well covered with TiO_2 [29] rich in terminal Ti-OH groups that play a role of the grafting sites during the chemical modification, for both silanization [1] and phosphonation [3]. The average composition of the surface, according to EDS analysis, was 7 at.% C, 61 at.% O and 31 at.% Ti, which indicates the important level of surface oxidation and the presence of some organic pollution.

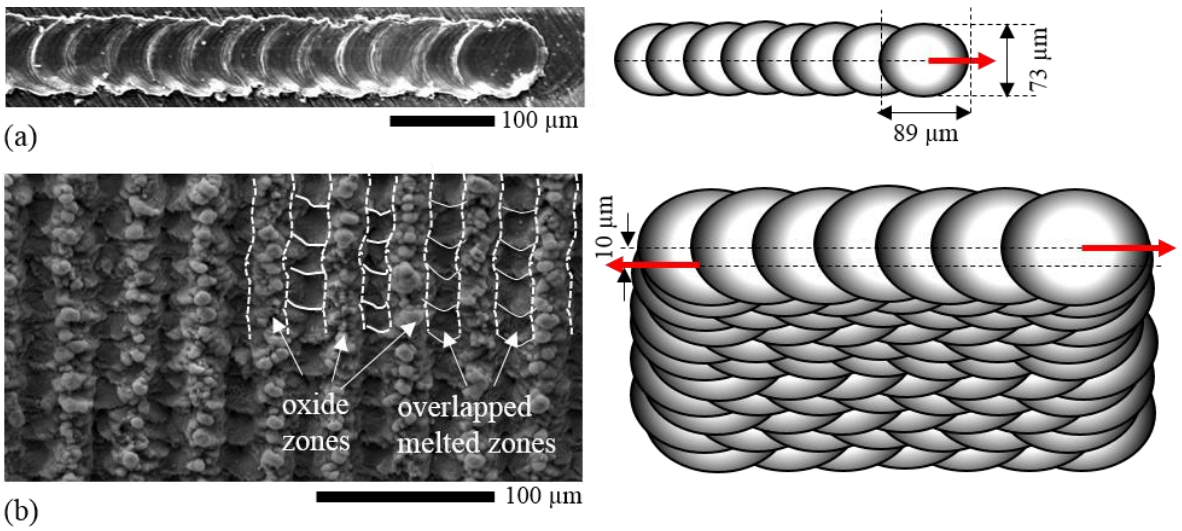

Figure 1. SEM topography views (on the left) and overlap schemes (on the right) of a standalone scanning line (a) and the topography obtained with 10 µm offset between the scanning lines (b).

The laser-treated samples had a light blue shade and were covered with white oxide particles, mostly composed by rutile (see the results of XRD and Raman spectroscopy in the *Supplementary material file*). The SEM observation (Figure 2a) and EDS analysis of the surface showed:

- clusters of spherical oxide particles with EDS composition of 8 at.% C, 72 at.% O and 21 at.% Ti;
- thin granular microstructure in the overlapped melted zones containing 3 at.% C, 42 at.% O and 55 at.% Ti.

To remove these weakly adhered particles, the laser-treated samples underwent US cleaning that revealed a highly irregular granular surface (Figure 2b) composed in average by 7 at.% C, 64 at.% O and 29 at.% Ti, which indicated the preservation of an oxide layer with the stoichiometry close to TiO_2. For comparison, the native polished titanium surface contained 89 at.% Ti, 11 at.% O and minor pollution of Si.

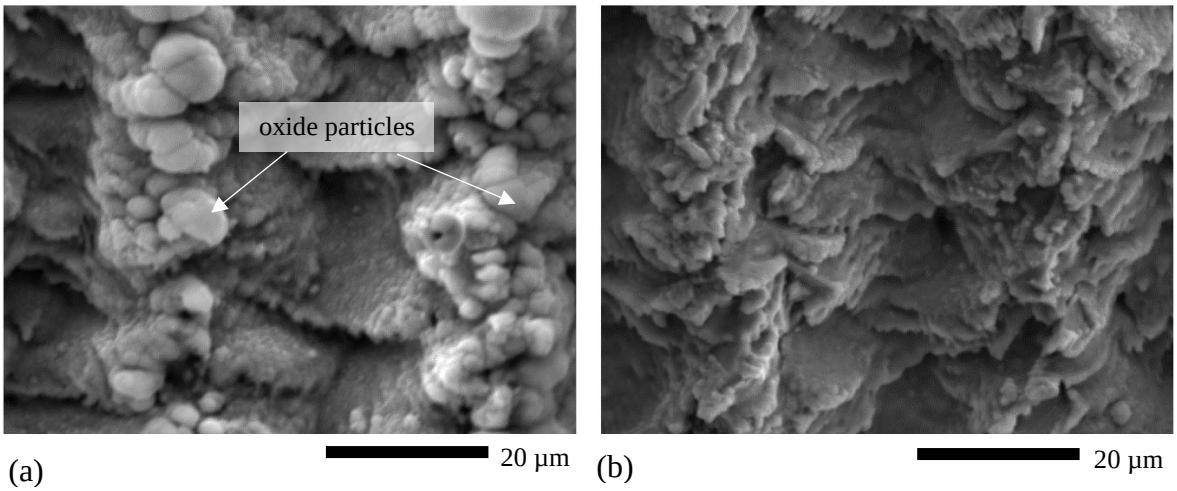

Figure 2. SEM topography view of the laser-treated surface before (a) and after (b) the US cleaning.

The cross section along the scan direction showed a wavy structure with a maximum difference between high and low points about 5-6 µm (Figure 3a). As no gas protection was used during the laser treatment, high local temperatures produced complete oxidation of the melted layer. The in-depth oxygen distribution (Figure 3b) allows roughly estimating the thickness of the titanium oxide layer to ~4 µm, which corresponds to an oxygen concentration higher than 33 at.% according to O-Ti phase diagram [31]). The XRD analysis of the laser-treated sample (given in *Supplementary information* file)

indicated the presence of α-Ti below the oxide layers, which is in agreement with stabilizing effect of dissolved O on α-Ti [31].

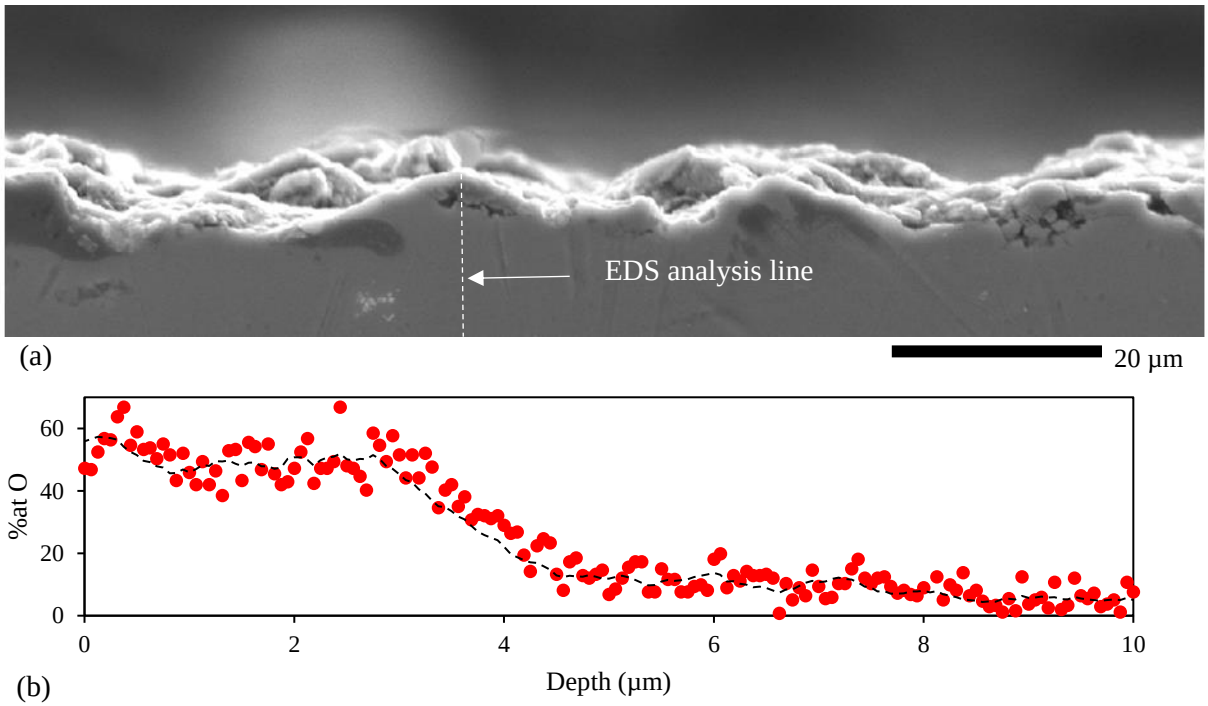

Figure 3. Cross section of a laser-treated substrate along the direction of the scan lines (a) and the distribution of O in depth according to EDS analysis (b).

Raman analysis of the US-cleaned surface (Figure 4) indicated the presence of anatase (A) with traces of rutile (R). In some places, standalone white oxide particles remained on the surface. These particles were mostly composed by rutile, the most stable TiO_2 form at high temperatures [32], and some addition of anatase. The identification of anatase and rutile peaks was done based on the reference values of vibrational frequencies provided in [33] and [34] respectively.

Anatase is a metastable form of TiO_2, and its dominant formation can be attributed to the rapid thermal gradients associated with nanosecond laser processing. On the other hand, rutile is thermodynamically stable and irreversibly forms from anatase at 600-700°C [35]. It is generally admitted that the initial TiO_2 phase formed during the oxidation of titanium is anatase, and its transformation into rutile is associated with grain coarsening process to the detriment of surrounding anatase [35]. The formation of vertical lines composed by the clusters of spherical rutile particles (Figure

1b, Figure 2a) can be explained as follows. Along with a violent oxidation, the action of laser pulse on the metallic surface produces a melted layer that is radially expulsed to the periphery of the impact zone due to the action of recoil pressure. This convection movement gives rise to the crests observed on the sample surface and brings coarse rutile particles at the borders of the melt, while thinner anatase layer remains all over the impact zone. The vertical lines of rutile particles perpendicular to laser scan direction are created by the overlap of the melted zones of the neighboring scan lines. Moreover, during the laser pulse, numerous micrometric droplets are ejected from the melt. Due to the extremely hot ambient temperature above the impact zone, some of these particles may also be transformed into rutile and fall on the periphery of the impact zone, where they can partially plunge into the melt or just remain weakly adhered to the roughened surface.

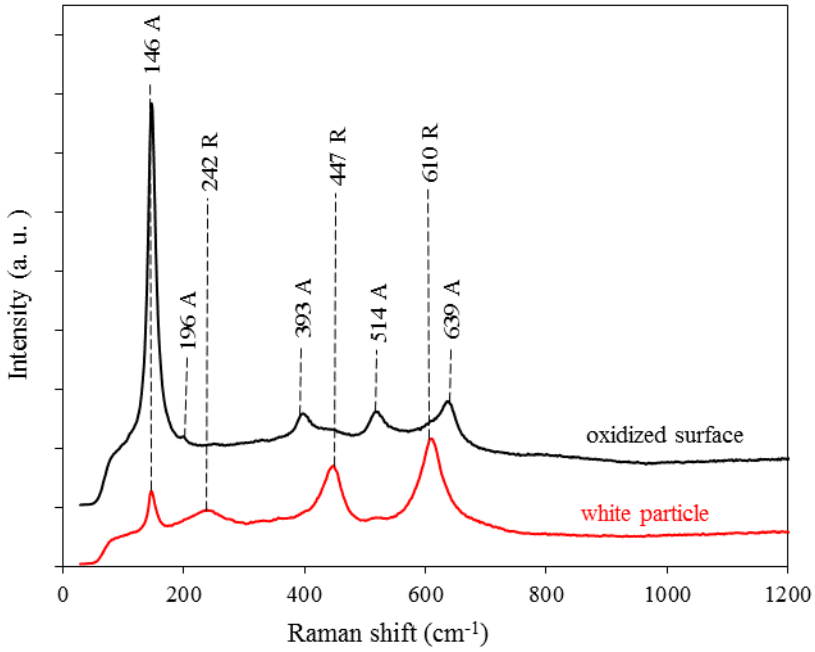

Figure 4. Raman analysis of the laser-treated surface after US cleaning. Legend of Raman vibrations: A - anatase, R – rutile.

Prior to chemical functionalization, the nature of the obtained surface was characterized by XPS using two different X-ray sources. The conventional Kα1 Al source that covers the binding energies up to 1400 eV, allowed identifying the elements composing the first 2 nm of the surface thickness (Figure

5a): Ti (with visible LMM, 2s, 2p, 3s and 3p peaks), O (KLL, 1s and 2s peaks) and C (KLL and 1 s peaks). On the other hand, the novel hard X-ray source Kα1 Cr (rarely reported in literature) allowed exploring higher binding energies up to 5000 eV (Figure 5b), that make visible additional 1s, KLL and KLM peaks for Ti and KLL peak for O. Moreover, in case of using Kα1 Cr source, the thickness of the analyzed surface extends to 6 nm, which makes it easier to get the signal from TiO_2 surface covered with a dense organic layers, as will be discussed in the sections *3.2* and *3.3*.

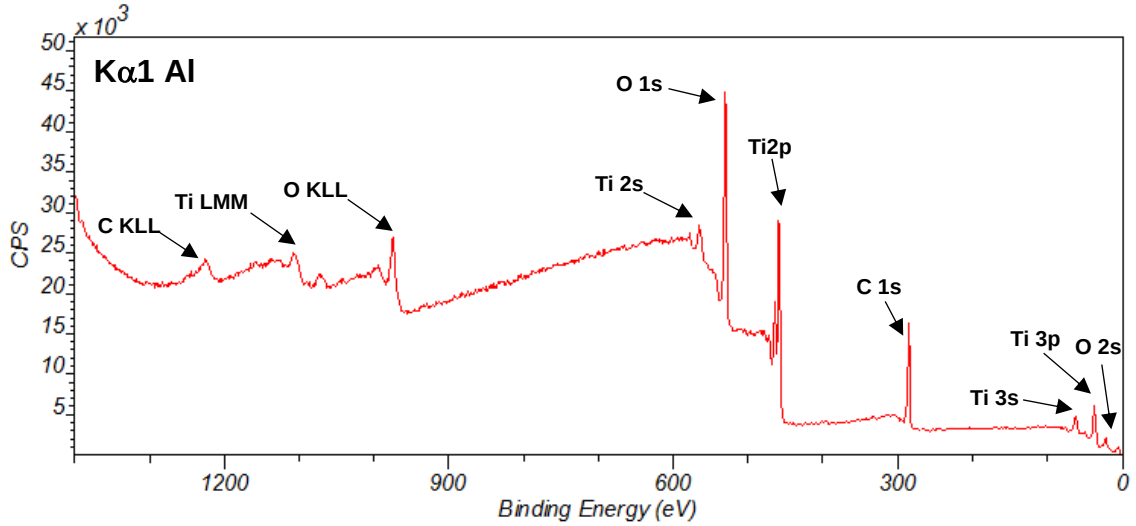

(a)

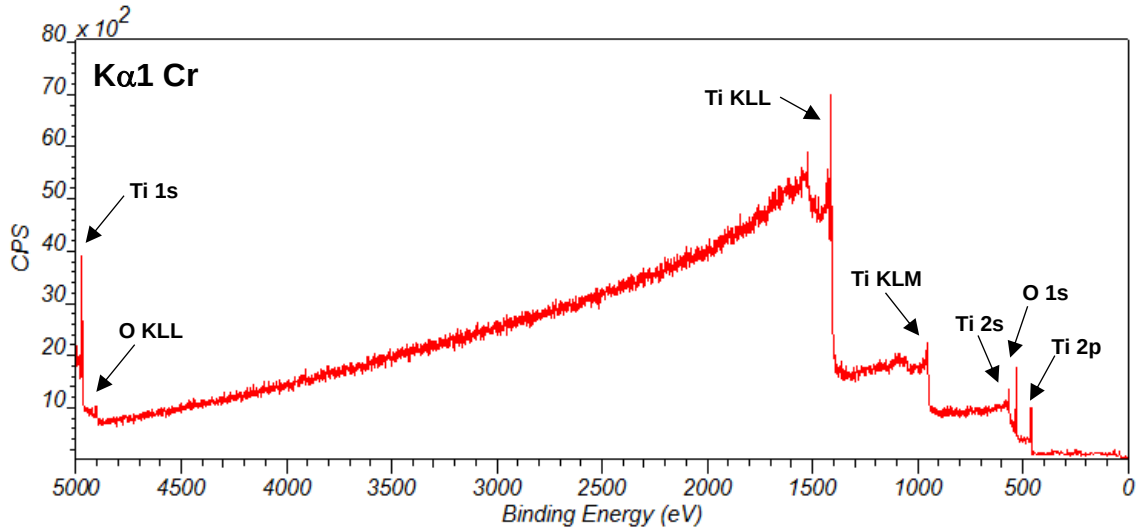

(b)

Figure 5. Survey XPS spectra of laser-treated US-cleaned surface obtained with (a) Kα1 Al and (b) Kα1 Cr sources.

Quantitative XPS analysis of the laser-treated surface using Kα1 Al (Table 1) showed that the US cleaning led to the complete removal of P and Si impurities and to the decrease of environmental organic pollution. The Ti:O ratio higher than 2 indicates the presence of some O-containing impurities. On the contrary to the existing literature [18,19,29,36], in given conditions of laser treatment, no N insertion was detected on the sample surfaces. This can be explained from one hand by the use of 532 nm Nd:YAG laser radiation that minimizes N insertion compared to commonly used 1064 nm [29], and from other hand by the difficulty to obtain XPS signal from the N-rich zone situated several nm below the superficial oxide layer [36].

Table 1. Elemental XPS analysis (at.%) of the laser-treated titanium before and after US cleaning.

at.%	Source	C	O	Ti	Si	P
Before US	Kα1 Al	31.7	54.2	13.1	0.5	0.5
After US	Kα1 Al	28.1	52.3	19.6	-	-
After US	Kα1 Cr	18.6	58.4	23.0	-	-

Comparison of the quantitative results obtained with Kα1 Al and Kα1 Cr sources on the US-cleaned surface (Table 1) showed a lower contribution of C in the case of Kα1 Cr, which is in agreement with the increased probe penetration. It is interesting to note that these quantitative results are very different from the EDS analysis, where the probe penetration is ~2 μm (according to Castaing formula [37]). As the oxide layer extends to ~ 4 μm (Figure 3b), both EDS and XPS probes do not reach the metallic substrate. Whereas EDS analysis approaches the stoichiometry of TiO_2 and estimates the C pollution at 7 at.%, both XPS sources give much higher O and C concentrations (Table 1). This difference is due to the following reasons: 1) the shallow depth of the XPS analysis makes it more sensitive to the environmental organic pollution of the surface than the EDS analysis for which the probe depth can reach several microns; 2) the EDS detector was operating at rather high acceleration voltage (20 kV) that creates maximal probe penetration; 3) the accurate quantification of the light elements such as C and O by common EDS detectors is very difficult because of the inaccuracy of the absorption correction and large variations in background, whereas it is possible with XPS analysis.

The detailed analysis of high-resolution XPS spectra of the identified elements provides important information on the nature of chemical bonds present on the laser-treated surface after US

cleaning. High-resolution XPS Kα1 Al spectrum of C 1s (Figure 6a) was composed by the following components: 78.5 % C-C and C-H (284.78 eV), 11.1% C-O (286.48 eV) and 10.4 % C=O (288.63 eV). High-resolution spectrum of O 1s (Figure 6b) contained 66.5 % TiO_2 (529.80 eV) and 31.5 % Ti-OH (531.56 eV) components along with 2% of H_2O and C=O pollutions (533.56 eV). High-resolution spectrum of Ti $2p_{3/2}$ (Figure 6c) was composed by 96 % of Ti(IV) of TiO_2 (458.49 eV) and by 4 % of sub-stoichiometric oxides TiO_x (456.82 eV).

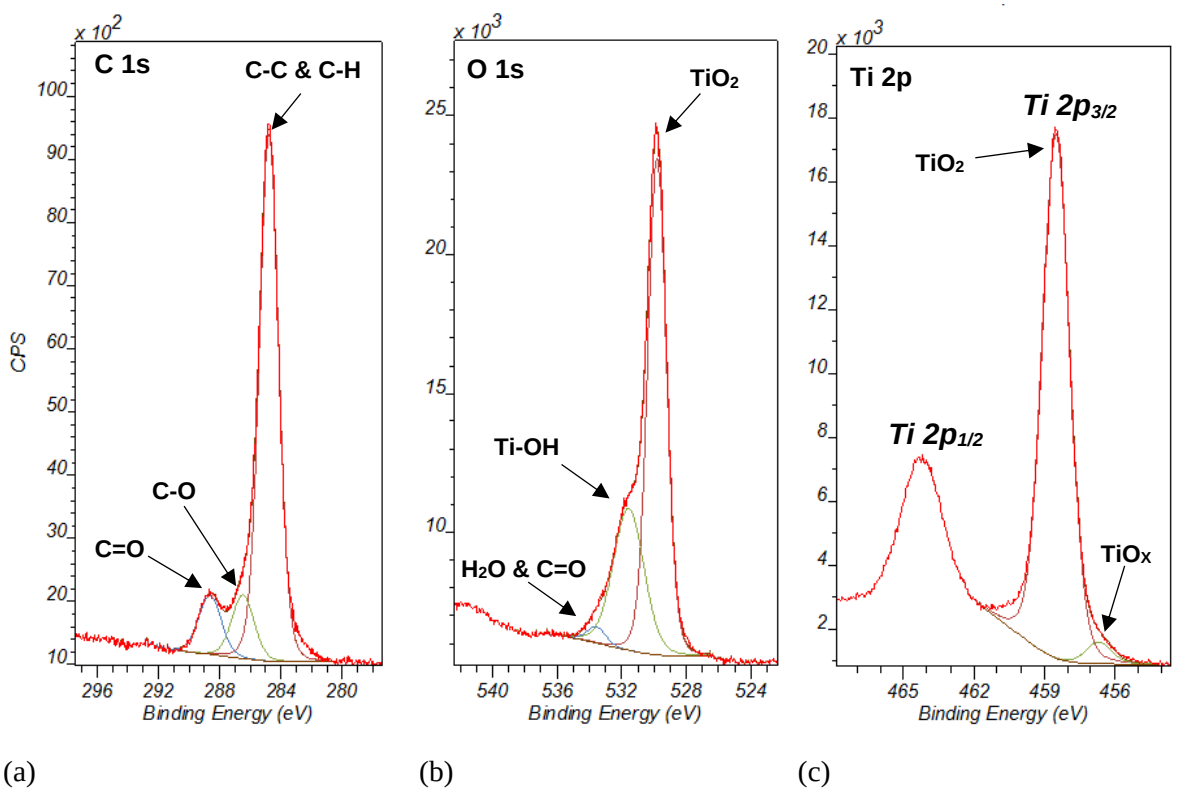

(a) (b) (c)

Figure 6. XPS Kα1 Al analysis of laser-treated substrate after US cleaning: high-resolution spectra of C 1s (a), O 1s (b) and Ti $2p_{1/2}$ and $2p_{3/2}$ (c) components.

On the other hand, high-resolution XPS Kα1 Cr probe provided the following results. Due to lower peak quality, a single C-C & C-H component at 284.79 eV was discernable for C 1s. For the same reason, only Ti(IV) TiO_2 (458.64 eV) component was observed in Ti $2p_{3/2}$ spectrum. Additionally, a single component at 4968.54 eV was observed in Ti 1s spectrum, which also can be attributed to Ti(IV) TiO_2. The components of O 1s were similar to those obtained with Kα1 Al: 76 % TiO_2 (530.17 eV), 18

% Ti-OH (530.97 eV) and 6 % of H_2O / C=O (532.10 eV). It can be concluded that the wavy TiO_2 surface bearing Ti-OH groups obtained after US cleaning is suitable for the covalent chemical functionalization.

The measurement of static contact angle is useful for evaluating the effect of laser treatment and further chemical functionalization on the wetting properties of the surface. Several works report that nanosecond [12,38] and femtosecond [39,40] laser treatments of titanium alloys in ambient atmosphere produce oxide layers with contact angles that evolve in time. Right after the processing, the laser-treated surfaces show hydrophilic behavior with contact angles 20-80° determined by the nature of TiO_2 layer covered with native -OH groups, while after several weeks the wetting angle reaches 120-160°, which is attributed to the progressive adsorption of airborne organic molecules containing hydrophobic alkyl chains. The presence of C-O, C=O and the intense C-C/C-H components in the C 1s XPS spectrum of the aged laser-treated sample (Figure 6a) indicates the pollution with O-containing compounds usually present in urban environments, such as alcohols, carbonyls, furans etc. [41, 42, 43]. The detection of C-O bonds can also be attributed to the adsorption of ethanol molecules during the US cleaning of the sample (see section *2.2*). It can be supposed that the O-containing groups interact with initially hydrophilic TiO_2 surface, while the organic chains are oriented externally and can eventually promote the secondary adsorption non-polar alkane, terpene or aromatic molecules that are the most frequent air pollutants across the world [42,44,45]. In the present work, the measurements of static contact angles were carried out several months after the laser processing and US cleaning in ethanol, which means that the final value of contact angle was already established, and for this reason the hydrophobic behavior was observed for laser-treated surfaces. In further work, the conservation time between the production of the laser-treated surfaces and their chemical modification should be reduced to diminish the adsorption of impurities, or the samples should be conserved in vacuum.

The initial surface of polished titanium was found hydrophilic (62°, in agreement with 61.5°[40] and 67.8°[11] reported for untreated Ti-6Al-4V and 63.1° obtained on commercially pure titanium [10]), whereas the laser-treated surface showed the superhydrophobic behavior with contact angle of 162°. However, after ultrasound cleaning (which was not performed in the above-cited works) the contact angle of the laser-treated surface diminished down to 138°, which can be attributed to the reduction of

the surface roughness due to the removal of weakly adhered and free oxide particles (Figure 2), in agreement with Wenzel wetting model [46].

3.2. Silanization experiments

Three tested approaches to grafting of silane molecules onto the oxidized titanium surface resulted in quite different organic loadings. The evaluation of grafting efficiency was made using XPS spectra obtained with XPS Kα1 Al (Table 2), where the presence of alkylsilanes on the sample surface is shown by the increase of C 1s peak and the appearance of Si 2s and Si 2p signals (Figure 7a). According to XPS Kα Al analysis, grafting in vapor phase at 170°C (sample Si-V) resulted in maximum Si loading of 10 at.%, whereas grafting in pure silane at 90°C (sample Si-D) resulted in smaller amount (5.9 at.% Si).

Table 2. Elemental XPS analysis of the functionalized substrates after different silanization experiments.

at.%	C	O	Ti	Si	Si:Ti	C:Si	Source
Si-S	33.2	50.1	16.4	0.3	0.02	0.01	Kα1 Al
Si-V	64.5	24.0	0.6	10.9	18.17	5.92	Kα1 Al
Si-D	72.9	18.7	2.5	5.9	2.26	12.36	Kα1 Al
Si-D	63.8	22.6	5.9	7.7	1.31	8.28	Kα1 Cr

The chemical functionalization in THF solution at 66°C (sample Si-S) was inefficient, with very low amounts of Si and the C loading close to that of the initial carbon pollution (Table 2). For this reason, the sample Si-S was not characterized further. This result can be explained by the insufficient chemical affinity of alkoxysilanes to TiO_2 and by the possible negative effect of accumulated airborne organic pollutants. The future attempts of synthesis in organic solvents should be made with freshly obtained oxide layers and using more reactive modifiers such as chlorosilanes [47].

For both Si-V and Si-D samples, the stoichiometric proportions C:Si (12:1 and 18:1 for ODTMS and DDTES silanes) were not respected. The observed understoichiometric C:Si ratios of 6:1 and 12:1 for Si-V and Si-D, respectively, reflect the attenuation of the signal of the Si-bearing anchor groups by long C_{12} and C_{18} carbon chains due to the limited inelastic mean free path of electrons crossing the organic layer [1]. This observation is in agreement with the low content of Ti obtained for the samples Si-V and Si-D compared to the sample Si-S. The titanium content is slightly higher for the sample Si-D

that has lower organic loading and shorter carbon chains (C_{12}) compared to Si-V (C_{18}). A Si:Ti ratio of 18.2 for Si-V sample indicates the formation of well-developed homocondensed silane layer. The Si:Ti ratio of only 2.4 for Si-D sample also indicates the homocondensation of silanes, however, much less pronounced due to lower temperature and time of the functionalization. A Si:Ti ratio of only 0.02 for Si-S sample indicates an incomplete monolayer coverage of the surface.

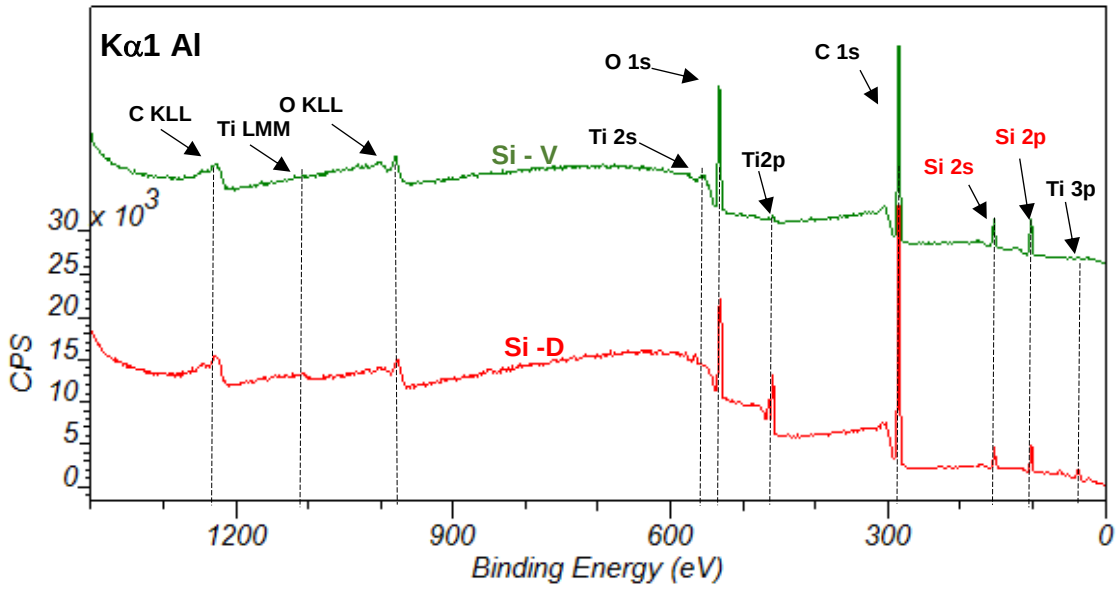

(a)

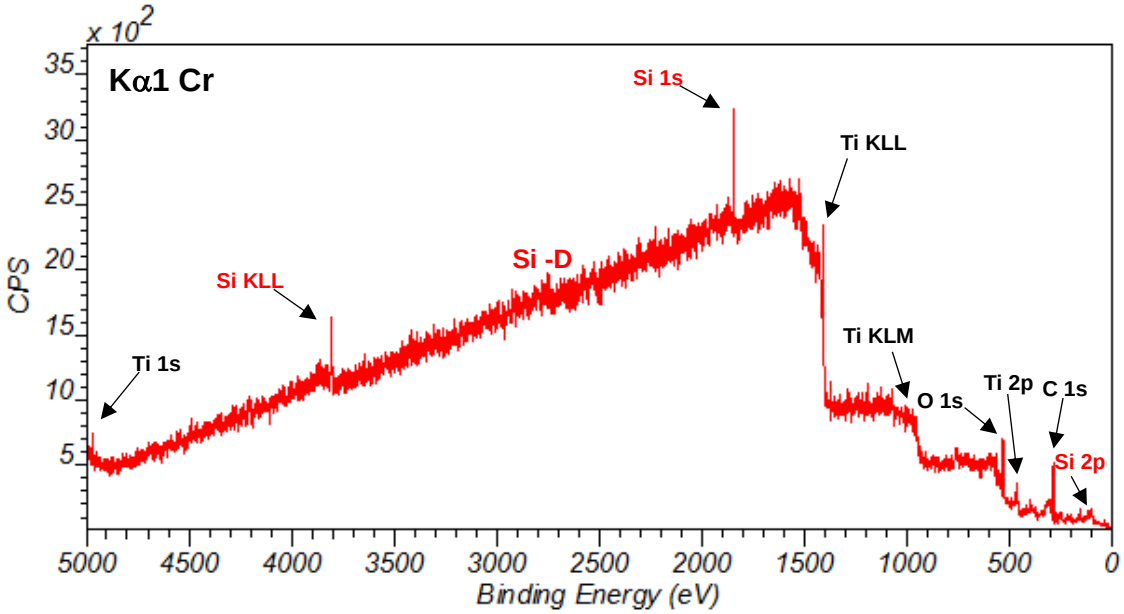

(b)

Figure 7. Survey XPS spectra of silanized samples obtained with (a) Kα1 Al and (b) Kα1 Cr sources.

The use of a Kα1 Cr probe for the analysis of the sample Si-D allowed a better detection of Ti and Si atoms situated on the surface shielded by organic chains (Table 2). However, the C:Si ratio (8.3) did not reach its theoretical value and Si:Ti ratio (1.3) still indicates rather low level of homocondensation of silanes. It is remarkable that the Si 2p peak has much lower quality than in Kα1 Al spectrum (Figure 7b) and is not suitable for the component analysis. On the other hand, an intense Si 1s peak of 7 eV width was observed at 1841.50 eV. A weak peak of Si KLL was also observed.

A high-resolution Si 2p spectrum of the sample Si-V obtained with Kα1 Al probe (Figure 8) showed the presence of very large (total width of 8 eV) peak centered at 102.75 eV corresponding to the presence of Si-containing groups with different chemical environments [1]. This observation supports the hypothesis about the well-developed polycondensed layer, where a part of Si-bearing anchoring groups reacted with Ti-OH surface groups to form Si-O-Ti bonds, whereas the part of them homocondensed and formed Si-O-Si bonds. The sample Si-D analyzed using Kα1 Al showed a slightly thinner peak (total width of 6eV) centered at 101.94 eV (Figure 8), which indicates lower diversity of Si environments. This is in agreement with the hypothesis of a less developed polycondensed layer, where a higher share of silane molecules reacted with Ti-OH surface groups (since Si-O-Ti bond corresponds to 102 eV [1]).

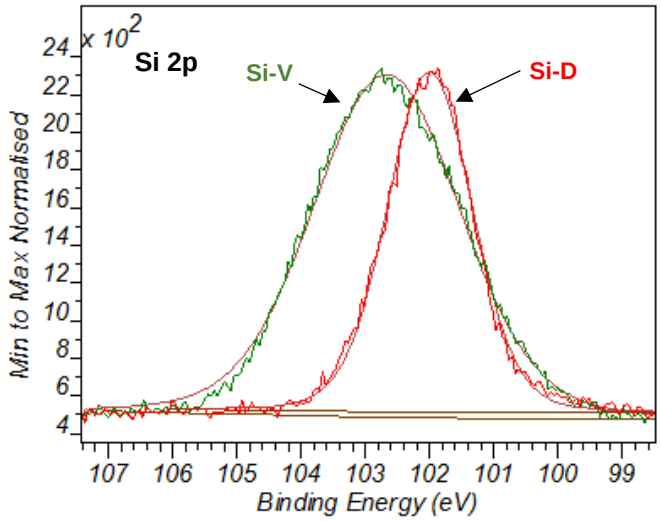

Figure 8. High-resolution Si 2p spectra of the silanized samples obtained using Kα1 Al.

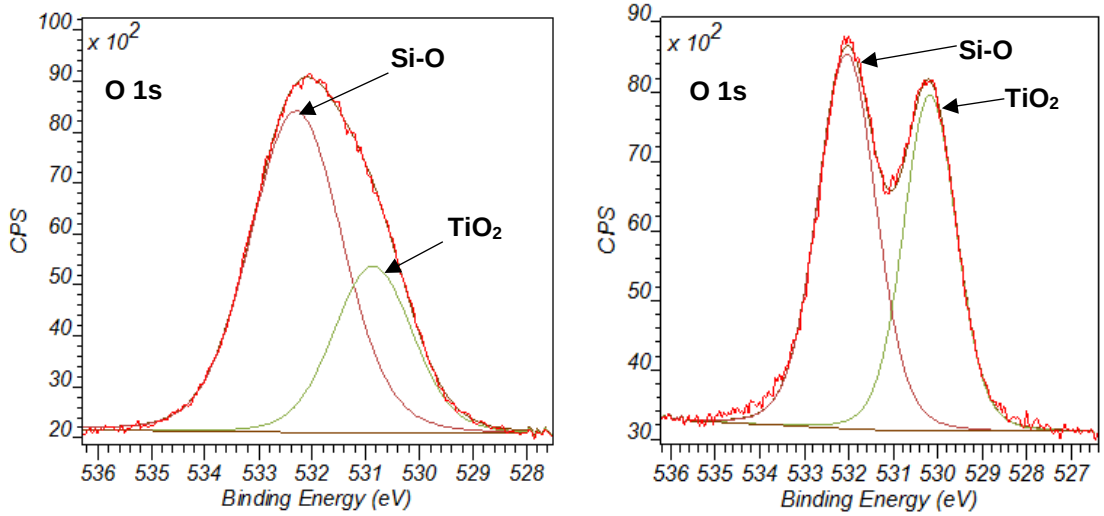

Figure 9. High-resolution O 1s spectra of the samples Si-V (a) and Si-D (b) obtained using Kα1 Al.

A high-resolution Ti 2p spectrum of the sample Si-V obtained using Kα1 Al was composed by 91 % of TiO_2 (459.61 eV) and by 9 % of sub-stoichiometric TiO_x (457.82 eV) components, while the sample Si-D showed 94 % TiO_2 (458.77 eV) and 5 % of sub-stoichiometric TiO_x (457.4 eV), similar to the initial laser-treated substrate. The spectrum obtained with Kα1 Cr had very low intensity and showed only one TiO_2 (458.67 eV) component. Moreover, a single peak at 4968.54 eV was observed for Ti 1s, similarly to the oxide layer before silanization (see section *3.1*), however the peak width slightly increased, possibly due to the establishment of Ti-O-Si bonds.

A high-resolution O 1s spectrum of the sample Si-V obtained with Kα1 Al (Figure 9a) contained two components, where that at 532.5 eV (73%) can be assigned to Si-O bonds (according to [48]) and that at 530.17 eV (21%) is attributed to Ti-O bond in TiO_2 [6]. Such proportion reflects the presence of a developed polycondensed silane layer. The sample Si-D showed the same components, but forming two distinct peaks (Figure 9b) : 55% Si-O and 45% Ti-O [6]. These components were also observed in the spectrum of Si-D obtained using Kα1 Cr probe, however, their intensity was inversed: 34.8 % for Si-O bonds (531.92 eV) and 61.7% for Ti-O bonds (530.15 eV) along with 3.5% H_2O pollution (533.17 eV). This change is in agreement with the higher penetration of the Kα1 Cr probe that increased the intensity of TiO_2 component situated under the grafted silane layer.

A high-resolution C 1s spectrum of the sample Si-V obtained using Kα1 Al contained 63 % C-C (284.80 eV) and 37% C-H (283.95 eV) components, which reflects the presence of C_{18} alkyl chain. No C-O contribution from unreacted $–OCH_3$ groups was observed, possibly because of signal attenuation by alkyl chains. A high-resolution C 1s spectrum of the sample Si-D obtained using Kα1 Al contained 84% C-C (284.80 eV), 11.4 % C-H (283.81 eV) and 4.6% C-O (285.91 eV) components. A weak but present C-O component can be attributed to the lower thickness of grafted organic layer, when unreacted –OEt groups situated next to the surface become visible. The use of Kα1 Cr probe resulted in low intensity peak for C1s where only one component at 284.76 eV corresponding to C-H bonds could be identified.

Raman analysis of the sample Si-D prepared with silane droplet at 90°C (Figure 10a) showed in the region of 50-1000 cm^{-1} similar phases to the original laser-treated surfaces (Figure 4), with a majority of anatase and some rutile, in both high and low points of the surface. On the other hand, the sample Si-V treated with silane vapors at 170°C showed a partial loss of laser-induced oxide layer (Figure 10c). The spectrum showed the most intense peak of anatase at 146 cm^{-1} and a double hump in the region of 50-800 cm^{-1} indicating the presence of a mixture of sub-stoichiometric oxides [49]. This smoothening effect is also observable on the SEM images (Figure 11a). According to the O-Ti phase diagram [31], titanium dioxide does not exhibit any phase transition below 460°C, and the high temperature oxidation of titanium is observed above 600°C [50]. Thus, it can be concluded that no phase transformations could occur during the synthesis at 170°C. The partial loss of oxide layer can be due to the violent evaporation of the adsorbed species that are volatile at 170°C, such as residual ethanol used for US cleaning and various environmental pollutants.

The presence of low intensity peaks at 1300 cm^{-1} and 1437 cm^{-1} (Figure 10b) in the spectrum of silanized samples can be attributed to the twisting and bending vibrations of CH_2 groups [51]. In the 2000-3500 cm^{-1} region, Figure 10d shows the presence of CH_2 and CH_3 stretching signals [51] centered at 2903 cm^{-1} and having the similar intensity for high and low points of the samples. No other peaks specific to the grafted silane molecules were detected.

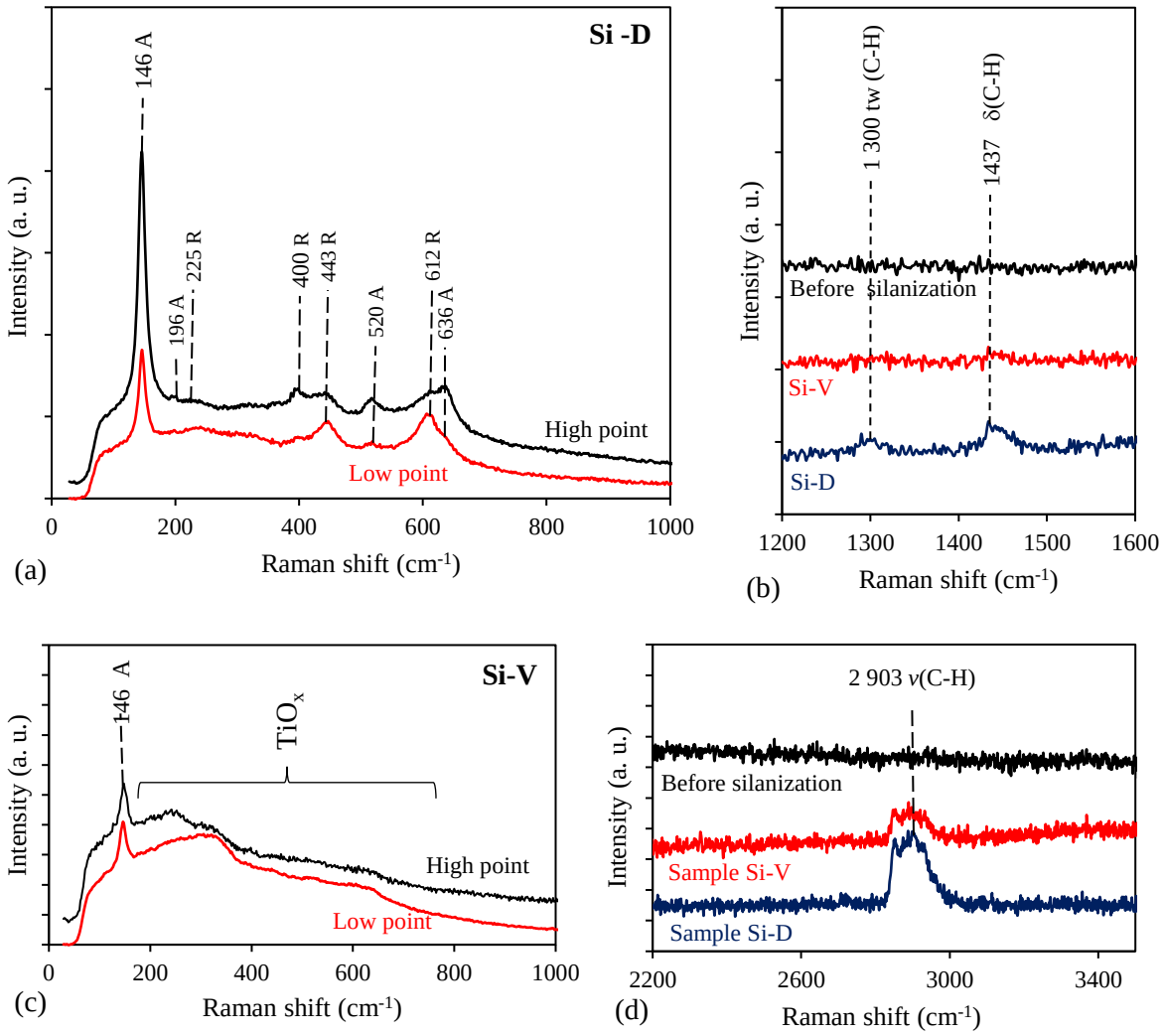

Figure 10. Raman spectra of (a) Si-D in 0 - 1000 cm^{-1} region; (b) 1200 - 1600 cm^{-1} region before and after silanization ; (c) sample Si-V in 0 - 1000 cm^{-1} region; (d) 2200-34000 cm^{-1} region before and after silanization. Legend of Raman vibrations: A - anatase, R – rutile, ν - stretching, δ - bending, tw – twisting.

The SEM observation of the sample Si-V (Figure 11a) confirmed the pronounced smoothening of the surface due to the partial loss of oxide layer indicated by Raman spectroscopy. The ratio between the average O and Ti contents issued from EDS and XPS analysis cannot be used for the appreciation of the oxide loss, since the additional oxygen atoms can be present on the surface in form of unreacted anchor groups of silane ($-OCH_3$). The variations of O and Si intensities along the direction of laser

displacement (Figure 11b) show the same tendencies as the signal of Ti, which signifies a simple topography effect on local intensity and not the preferential insertion of silane molecules at the low or at the high points of the substrate. The sample Si-D showed also a uniform Si insertion, however, the morphology of the surface was close to the state before chemical functionalization such as shown on Figure 2b.

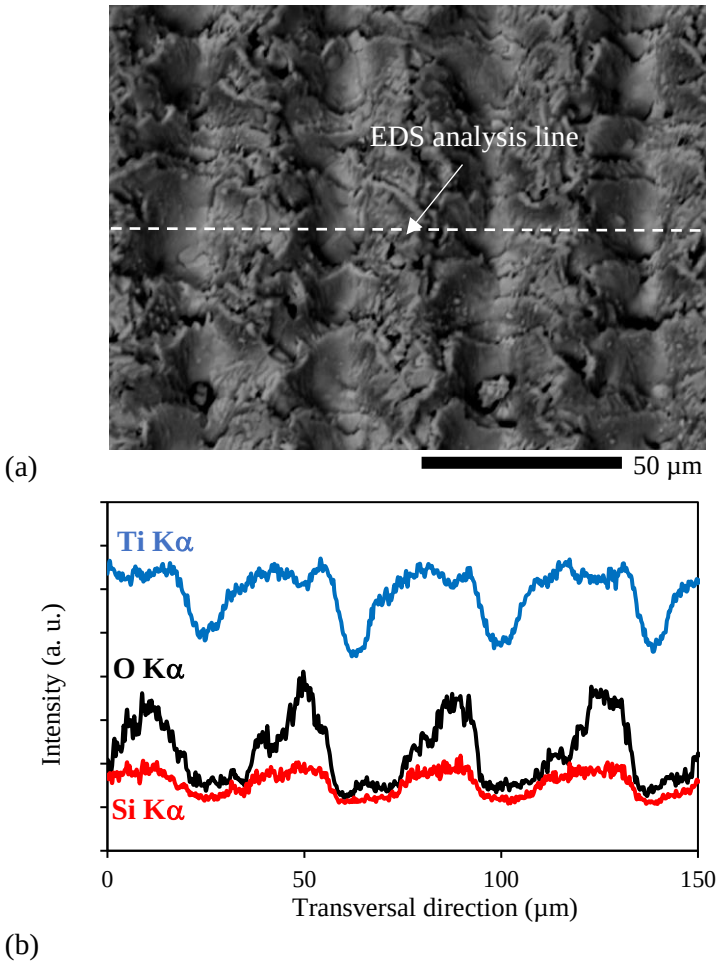

Figure 11. Topography SEM observation of the sample Si-V after chemical functionalization (a) and the distribution of Kα line intensities of Ti, Si and O along the laser scan direction (b).

The measurements of static contact angle showed the increase in hydrophobicity of the surface for both Si-V (142°) and Si-D (151°, Figure C in *Supplementary information*) samples compared to the US-cleaned laser-treated substrate (138°). The high organic load observed and the significant increase in the wetting angle for the silanized samples are encouraging for using this treatment in the production of self-cleaning hydrophobic surfaces and for the enhancement of adhesion strength of non-polar

polymers to titanium surfaces. Lower contact angle for the sample Si-V compared to Si-D, despite its higher organic load, can be attributed to the visible smoothening of the surface (Figure 11a) induced by severe conditions of chemical functionalization, in agreement with Wenzel model [46]. These results are comparable to the values reported in the recent publication of Guo et al. [11], where laser-treated Ti-6Al-4V surface was functionalized with trichloro(1H,1H,2H,2H-perfluorooctyl)silane by dipping in 1 mM solution and drying in the oven at 150°C for 1h. The authors reported that the maximum contact angle was observed for most rough surfaces (150°), lower value (145°) for the medium roughness and minimal value (104°) for the flat surface.

3.3. Phosphonation experiments

The XPS analysis using Kα1 Al source allowed detecting the presence of P atoms on the surface: P 2s and P 2p peaks were visible for the highest (P100) as well as for the lowest (P5.6) concentration of OPA (Figure 12a). Moreover, the intense peaks P 1s and P KLL were observed in survey spectrum of P100 obtained with Kα1 Cr (Figure 12b), whereas the P 2p peak was of poor quality.

According to XPS analysis using Kα1 Al probe, the use of solutions with increasing OPA concentration led to the progressive increase of P content followed by the saturation at ~7 at.%, starting from acid concentration of 50 mM (Figure 12n Table 3). It is remarkable that the double increase of OPA concentration from 50 to 100 mM did not bring a significant rise of P loading (+0.2 at.% P), which indicates the full coverage of the sample surface (since phosphonic acids undergo exclusively heterocondensation with formation of Ti-O-P bond [20]).

At the same time, the C loading on the surface showed a slow increase with OPA concentration (Figure 12, Table 3), except the sample P5.6 that obviously contains a significant ambient pollution. The C:P ratio of 9-12 was obtained for different samples (Figure 12, Table 3), which is higher than the theoretical ratio of 8 expected for OPA. This can be attributed, from one hand, to the presence of organic pollution, and from another hand, to the pronounced attenuation of P signal by the C8 chain, since P atoms are exclusively located on the surface, unlike the polycondensed silanes considered in section *3.2*. The hypothesis about the attenuation effect is also supported by rather weak signals of Ti and O obtained with Kα1 Al probe compared to the original laser-treated sample (Table 1).

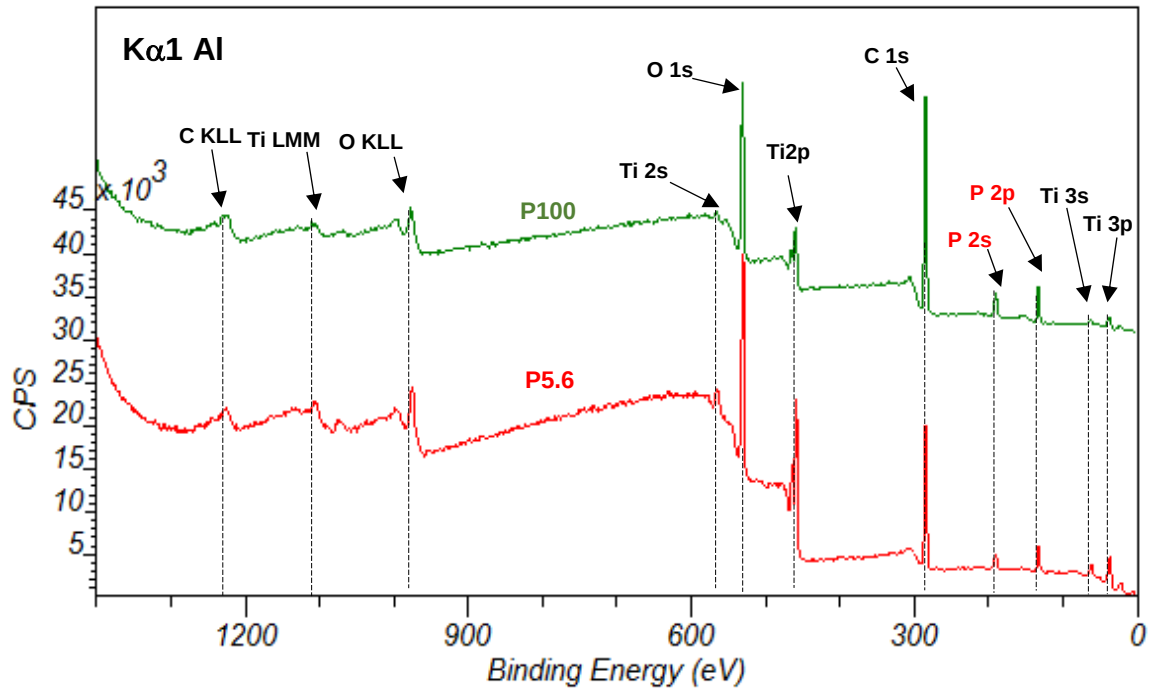

(a)

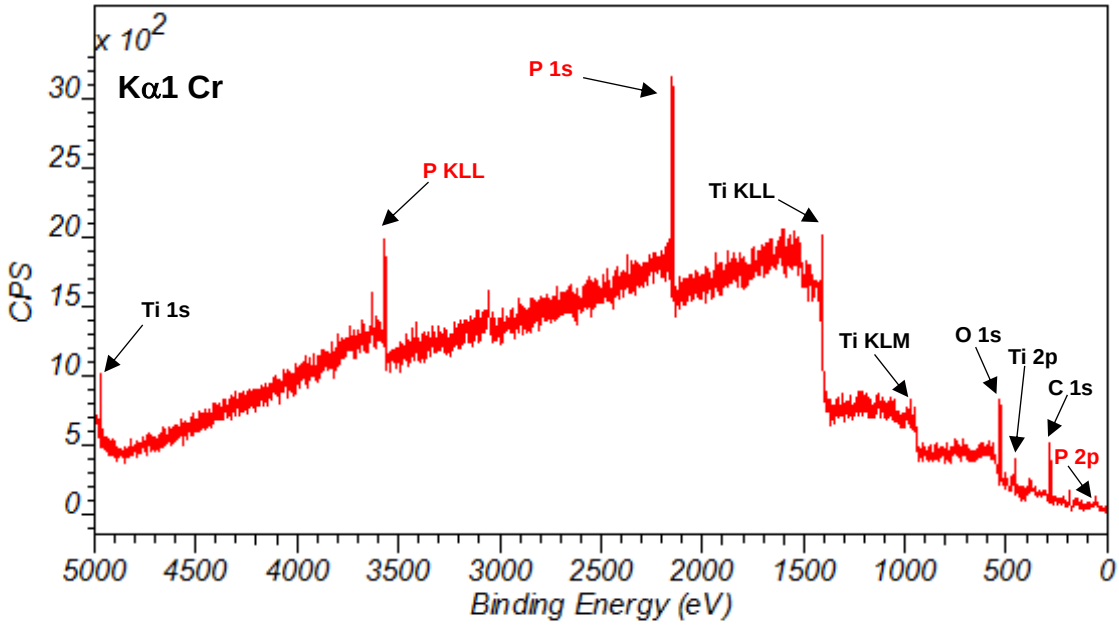

(b)

Figure 12. Survey XPS spectra of phosphonated samples (a) P5.6 and P100 obtained with Kα1 Al source and (b) P100 obtained with Kα1 Cr source.

Table 3. Elemental composition of the functionalized surfaces after phosphonation experiments in OPA solutions with different concentrations, according to XPS analysis.

Sample	C_{OPA} (mM)	at.%				P:Ti	C:P	Source
		C	O	Ti	P			
P5.6	5.6	60.2	31.1	3.8	4.9	1.29	12.38	Kα1 Al
P10	10	57.8	31.6	4.5	6.1	1.36	9.48	Kα1 Al
P16.8	16.8	60.7	29.6	3.5	6.2	1.77	9.79	Kα1 Al
P50	50	62.9	27.2	3	6.9	2.30	9.11	Kα1 Al
P100	100	63.8	26.5	2.6	7.1	2.73	8.98	Kα1 Al
P100		59.8	28.7	5.8	5.7	0.98	10.37	Kα1 Cr

The proportion between P and Ti progressively increased from 1.3 to 2.7 with OPA concentration. However, these values reflect the progressive monolayer coverage of the surface associated with increased shielding of Ti atoms by octylphosphonic molecules. This hypothesis is supported by the observed decrease of P:Ti ratio when using more penetrating Kα1 Cr probe (sample P100, Figure 12, Table 3). Thus, the obtained P:Ti values do not allow to draw a conclusion about the nature of dentation that would correspond to a proportion between Ti and P varying from 1 to 3.

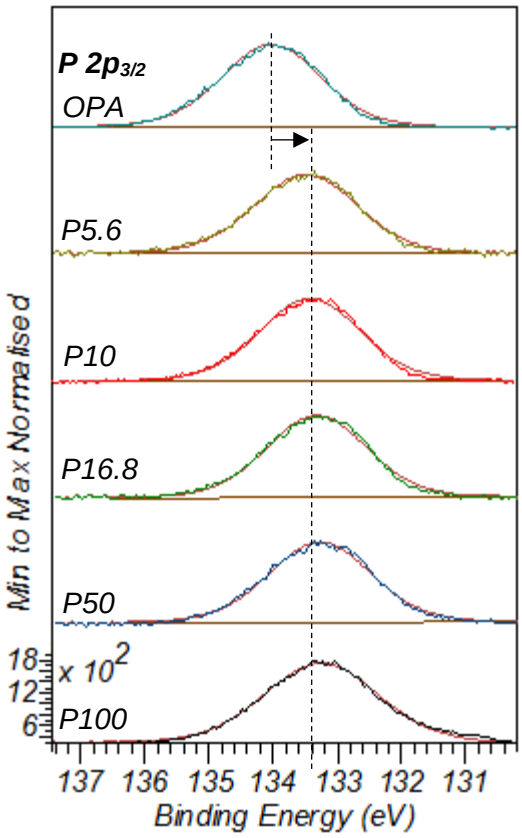

Figure 13. High-resolution P $2p_{3/2}$ spectra of pure OPA and phosphonated samples obtained with Kα1 Al probe.

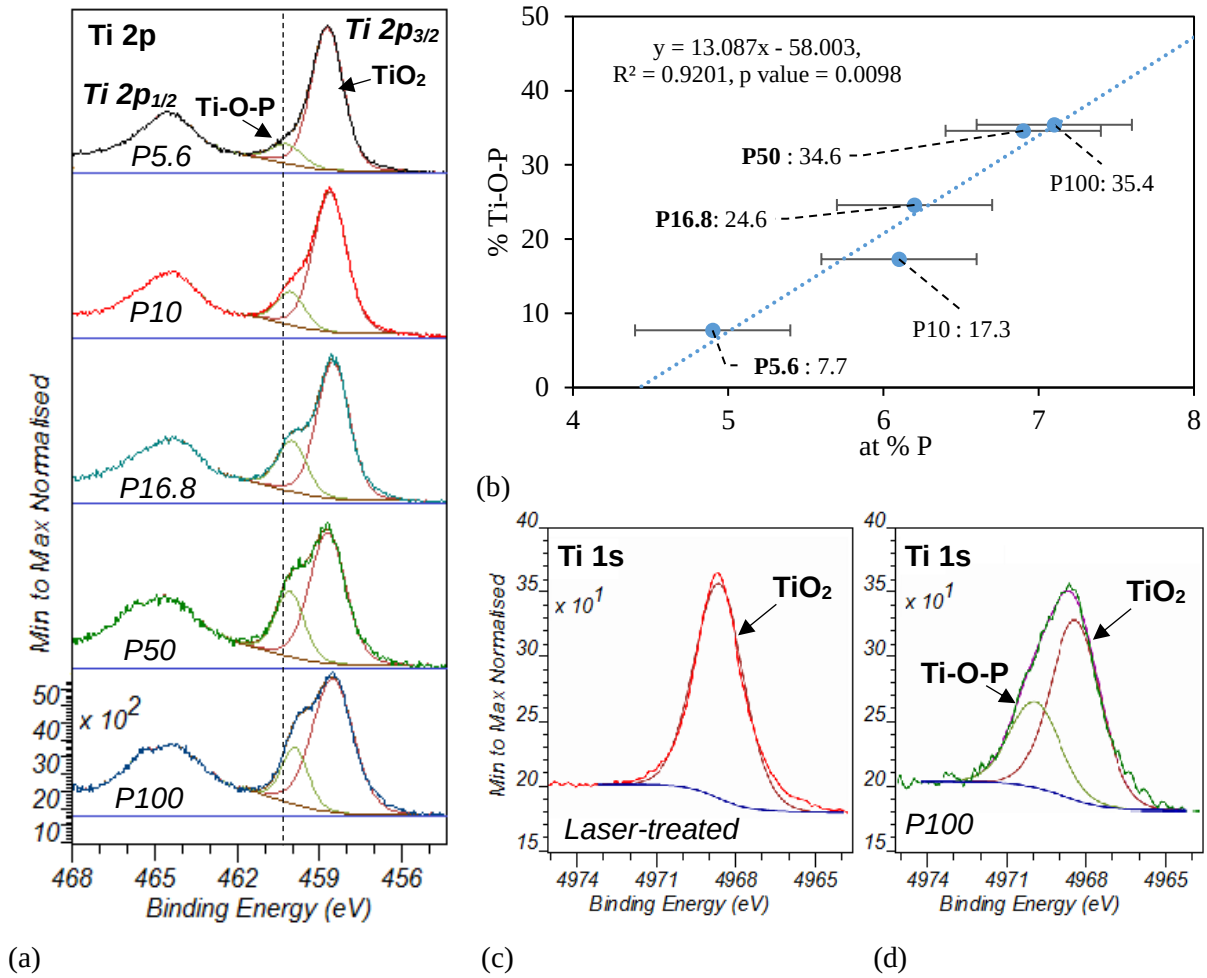

Figure 14. High-resolution Ti $2p_{3/2}$ spectra obtained with Kα1 Al probe for phosphonated samples (a) and the correlation between the abundance of Ti-O-P bonds (from Ti $2p_{3/2}$) in function of P content on the surface (b); the high-resolution Ti 1s spectra obtained using Kα1 Cr probe for the laser-treated sample before phosphonation (c) and for the sample P100 (d).

The high-resolution spectra of P $2p_{3/2}$ obtained with Kα1 Al probe (Figure 13) show a single component with full width at half maximum (FWHM) ~ 2 eV and a maximum between 133.42 (sample P5.6) and 133.17 eV (sample P100), whereas the determined binding energy in pure crystalline OPA is of 134.06 eV and FWHM ~1.8 eV. Such decrease (-0.64 to -0.89 eV) of binding energy of P can be explained by the creation of a covalent bond with surface Ti-OH groups. Similar shifts between P $2p_{3/2}$

signal in free and bonded octadecylphosphonic acid were reported for the grafting on the surface of TiO_2 (-0.2 eV [52]), Ta_2O_5 (-0.5 eV [53] and Ni-W (-0.8 eV [54]).

The high-resolution spectra of Ti $2p_{3/2}$ obtained with Kα1 Al probe were composed by two components with binding energies of 458.8 and 460.2 eV and equal FWHM of ~1.4 eV (Figure 14a). The intensity of the second component strongly correlates with the concentration of P on the surface (Figure 14b) with *p*-value <<0.05. The first component corresponds to Ti(IV) in TiO_2, whereas the second component can be attributed to the formation of superficial Ti-O-P bonds. This explanation is also in agreement with the decrease of the Ti-O-P component (459.89 eV) for the sample P100 from 35.4 % when using the Kα1 Al probe to 28.9 % when using the Kα1 Cr probe, as the deeper layer of TiO_2 is analyzed.

Moreover, the comparison of Ti 1s spectra of the laser-treated substrate before and after phosphonation (sample P100, Figure 14c-d) also indicates the creation of a new chemical environment: a new component centered at 4969.79 eV and having relative intensity of 32.4% appears after the phosphonation reaction, whereas the Ti 1s component of TiO_2 is situated at 4968.35 eV.

The high-resolution spectra of O1s obtained with Kα1 Al probe were composed by three components (Figure 15a): 529.90-530.10 eV, 531.22-531.47 eV and 532.80-533.20 eV. The same components were described in many studies on titanium alloys and titanium oxides functionalized with alkylphosphonic acids [5, 55,56, 57,58,59] that assign the 529.90-530.25 eV component to TiO_2, that of 531.2-531.6 eV to Ti-O-P bond and that of 532.6-533 eV to the protonated P-OH or P-O(···H)-Ti groups.

The O 1s spectra of the unbonded alkylphosphonic acids are composed, according to the literature [55,57], of 531.7-531.9 eV component corresponding to P=O group and 533.0-533.2 eV corresponding to P-OH. The proportion between these components in the unreacted acid (P=O/P-OH = 1:2) reflects the structure of OPA. In agreement with these results, the octylphosphonic acid used in this study produced the O1s peak composed by 531.77 eV component corresponding to P=O group (33 %at.) and 533.3 eV component corresponding to two P-OH groups (66 % at.). It can be noticed that the binding energies of Ti-O-P and P=O are very close, as well as P-OH and P-O(···H)-Ti.

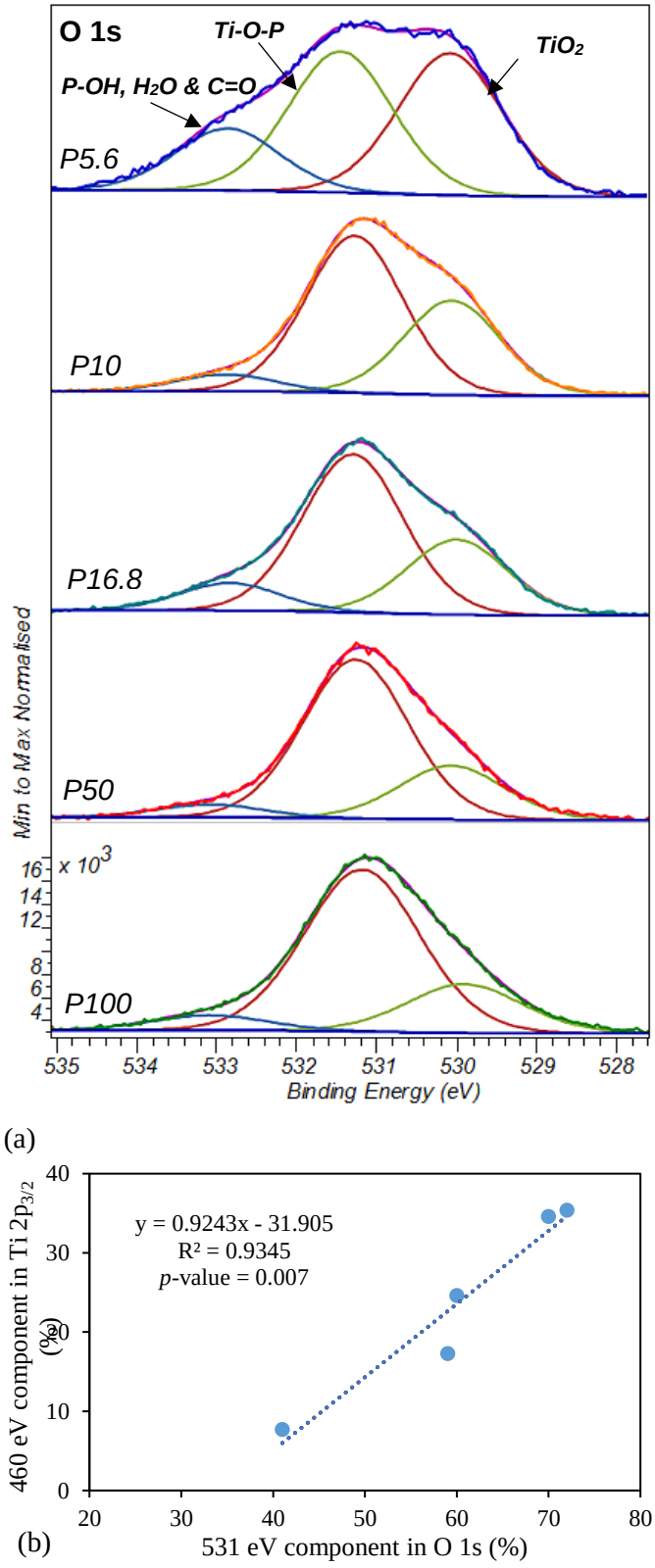

Figure 15. High-resolution O 1s spectra obtained with Kα1 Al probe for the phosphonated samples (a) and the correlation between the abundance of the components 460 eV Ti $2p_{3/2}$ and 531 eV O 1s attributed to the formation of Ti-O-P bonds (b).

The less energetic component at 529.9-530.1 eV attributed to TiO_2 progressively decreased from 41 to 21 %at. as the organic loading increased (Table 4). On the contrary, the second component (531.22-531.47 eV) attributed to Ti-O-P bonds (undifferentiated from P=O) increased with the concentration of OPA solutions up to 70% for the sample P50, but remained almost unchanged for P100 (Table 4). This indicates the formation of a complete self-assembled monolayer starting from an OPA concentration of 50 mM. Moreover, the integrated intensity of this component perfectly correlates (p-value <<0.05) with that of the 460 eV component of Ti $2p_{3/2}$ peak that is attributed to Ti signal from Ti-O-P bonds (Figure 15b). The third component at 532.8-533.2 corresponds to P-OH, but also to C=O bonds from the organic impurities and H_2O. For this reason, its relative intensity cannot be a direct indication of the quantity of unreacted P-OH groups. The samples P50 and P100 having complete SAM show the lowest intensities of this component (only 6-7%), which is possibly due to the replacement of the adsorbed impurities by grafted OPA molecules. For these samples, the ratio between Ti-O-P and P-OH&H_2O&C=O components neared 12:1, which indicates that at least 92% of P-OH groups were deprotonated as they reacted with TiO_2. The results obtained with Kα1 Cr for the sample P100 showed the same three components (Table 4). The increase of TiO_2 component compared to Kα1 Al reflected the higher analyzed depth in the oxide layer. A slight increase of P-OH&H_2O&C=O component with probe depth allows supposing that the residual P-OH groups and remaining impurities, comprising H_2O, are located near the TiO_2 surface and do not correspond to some unreacted OPA molecules retained in the organic layer by Van der Waals forces.

Table 4. The relative abundances of three components in high-resolution O 1s spectra of phosphonated samples: TiO_2 (529.90-530.10 eV), Ti-O-P (531.22-531.47 eV) and P-OH & H_2O & C=O (532.80-533.10 eV).

Sample	**C_{OPA} (mM)**	**% components**			**Source**
		TiO_2	**Ti-O-P**	**P-OH & H_2O & C=O**	
P5.6	5.6	41	41	18	Kα1 Al
P10	10.0	35	59	6	Kα1 Al
P16.8	16.8	30	60	10	Kα1 Al
P50	50.0	24	70	6	Kα1 Al
P100	100.0	21	72	7	Kα1 Al
P100	100.0	25	66	9	Kα1 Cr

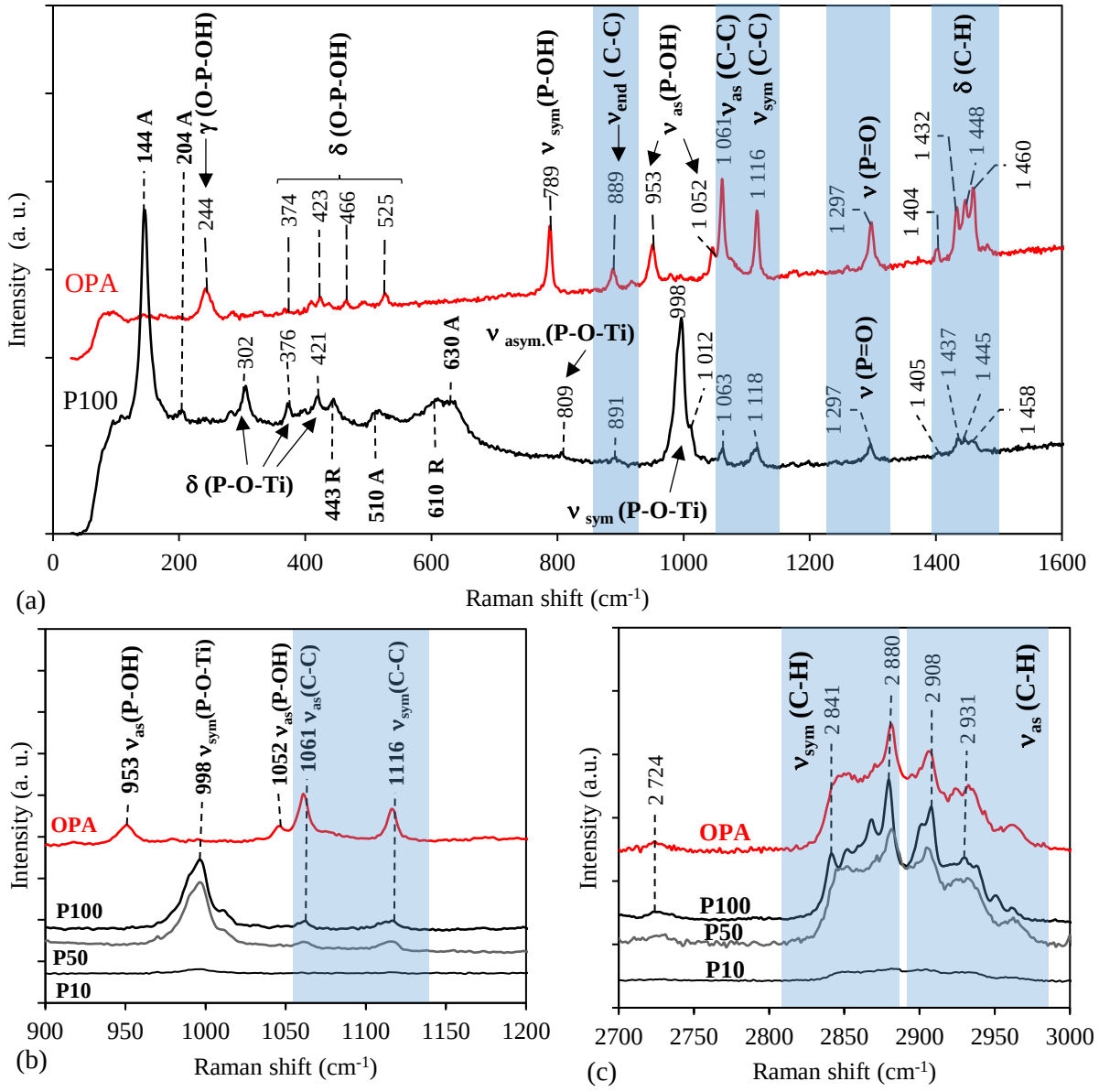

Figure 16. Raman analysis of the phosphonated samples: (a) comparison of OPA and sample P100 in 50-1800 cm^{-1} region; (b) various phosphonated samples in 900-1200 cm^{-1} region; (c) OPA and phosphonated samples in 2200-3400 cm^{-1} region. Legend of Raman vibrations: A - anatase, R – rutile, ν - stretching, δ - bending, γ - rocking, end – vibrations of terminal groups, sym – symmetric, as - asymmetric.

The high-resolution spectra of C 1s obtained with Kα1 Al probe contained in all cases a major (93-95%) C-C & C-H component (284.81-284.81 eV) along with a minor C-P [6] & C-O (286.46-286.79 eV) component. In case of Kα1 Cr probe, only C-C & C-H component at 284.70 eV was identified because of low peak quality.

Raman spectrum of the phosphonated sample with the highest loading of phosphonic groups (P100) was compared to the spectrum of native crystalline octylphosphonic acid (Figure 16a). In the low frequency range (<1000 cm^{-1}), the spectrum of the sample P100 was similar to that of the laser-treated samples (Figure 4), with the presence of the anatase and rutile vibrations. The assignment of vibrational frequencies of OPA and phosphonated samples was made on the basis of the literature describing the spectroscopic behavior of phosphonic groups (see *Supplementary material* file) and alkyl chains [60]. The unbonded phosphonic group $-PO_3H_2$ in OPA is characterized by the presence of a rocking vibration γ(O-P-OH) = 244 cm^{-1} that is absent in the spectrum of P100. This is the first indication of the very low amount of unreacted phosphonic groups on the surface. Four weak bending vibrations δ(O-P-OH) were observed at 374, 423, 466 and 525 cm^{-1} in the spectrum of OPA, whereas the spectrum of P100 contained stronger vibrations at different positions (302, 376 and 421 cm^{-1}), which can be attributed to the formation of P-O-Ti bonds.

For higher frequencies, the pronounced peak at 789 cm^{-1} in the spectrum of OPA can be assigned to the symmetrical stretching vibration ν_{sym}(P-OH), while the closest peak in the spectrum of P100 situated at 809 cm^{-1} is shifted and very weak. It can be possibly assigned to $\nu_{asym.}$(P-O-Ti) vibration. Asymmetrical stretching vibrations ν_{as}(P-OH) can be found at 953 and 1052 cm^{-1}, while in the spectrum of P100 they are replaced by an intense peak at 998 cm^{-1} with a shoulder at 1012 cm^{-1} that belong to the symmetric stretching vibrations of P-O-Ti bonds (ν_{sym}(P-O-Ti)). These vibrations were also detected in the samples P10 and P50 (Figure 16b). Vega et al. [61] observed similar strong peak with a weaker shoulder (1108 and 1080 cm^{-1} respectively) after the modification of SiO_2 with octadecylphosphonic acid (ODPA) and assigned it to the stretching vibrations of Si-O-P bidentate bonds. On the other hand, Hotchkiss et al. [62] attribute the similar broad peak at 1016 cm^{-1} with a shoulder to the stretching mode of PO_3^{2-} group of ODPA bonded to the surface of ZnO in tridentate mode. The absence of P-OH vibrations in the spectra of phosphonated samples discards the hypothesis about monodentate bonding of OPA and is in agreement with very weak P-OH component identified in O 1s XPS spectra (Figure 15, Table 4). At 1297 cm^{-1}, the stretching vibration of P=O group (ν(P=O)) can be observed in both OPA and P100, which allows dismissing the possibility of predominant tridentate bonding. Thus, it can

be concluded that the bidentate bonding mode prevails. Some other vibrations also did not change their position, but only lost in intensity compared to the original OPA. In the region 850-1150 cm^{-1} these were stretching C-C vibrations of the terminal methyl group (ν_{end}(C-C) = 889 cm^{-1}) as well as asymmetric (ν_{as}(C-C) =1061 cm^{-1}) and symmetric (ν_{sym}(C-C) =1116 cm^{-1}) stretching vibrations of C-C chains (Figure 16a-b). In the region of 1400-1460 cm^{-1}, several bending C-H vibrations (δ (C-H)) were present both in OPA and in P100 spectrum. Unattributed low intensity peaks were observed around 2724 cm^{-1} in both OPA and P100 (Figure 16c). Such weak peaks were also found in Ni-W samples modified with octadecylphosphonic acid [54], but with no interpretation. The intense peaks of symmetric (ν_{sym}(C-H) = 2843 and 2880 cm^{-1}) and asymmetric (ν_{as}(C-H) = 2907 and 2931 cm^{-1}) stretching C-H vibrations [61] were similar in OPA and in phosphonated samples (Figure 16c).

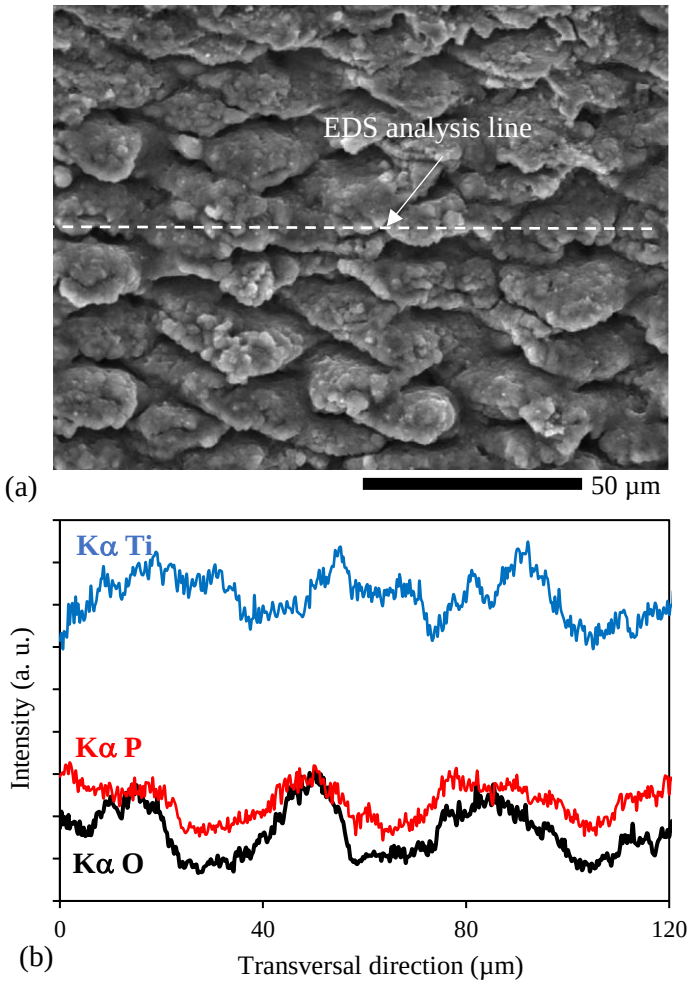

Figure 17. Topography SEM observation of the sample P100 after chemical functionalization (a) and the distribution of Kα line intensities of Ti, Si and O along the laser scan direction (b).

The EDS analysis of phosphonated surfaces showed uniform P distribution, which is in agreement with the formation of full phosphonic monolayers. The synthesis conditions did not seem to affect the initial roughness of the surface (Figure 17a), which is in agreement with the conservation of TiO_2 layer according to Raman spectroscopy (Figure 16a). The variations of O and P intensities along the direction of laser displacement show the same tendencies as the signal of Ti, which signifies a simple topography effect on local intensity and not on the local density of grafted groups (Figure 17b).

Static contact angle measurements showed the increase in hydrophobicity of the surface compared to the US-cleaned laser-treated sample (138°): from 144° for P5.6 (Figure D in *Supplementary information*) to 152° for P100, which is comparable to the hydrophobicity of the silanized samples discussed in the paragraph *3.2*. The literature analysis of metals and metal oxides modification by phosphonic acids generally reports lower values: 103° for decylphosphonic acid on aluminum [63], 120° of octadecylphosphonic acid (ODPA) on alumina [64], 120° and 130° for ODPA on stainless and carbon steel [65], 101° for ODPA on Co-Cr alloy [66], 100° for hexadecylphosphonic acid on Ti45Nb alloy [67] and 110° for ODPA on titania [68]. However, these were obtained on unstructured surfaces and with lower (typically 1 mM) concentrations of the modifier.

Beyond the effect on the hydrophobicity of metallic titanium surfaces, a nanosecond laser treatment followed by chemical functionalization with long organic chains would be a way to develop efficient inorganic-organic interfaces when joining or coating titanium alloys with polymers. To this end, the relative importance of two different effects has to be studied: 1) the effect of the laser-induced surface patterning on the metal-polymer mechanical interlocking and, 2) the chemical affinity of the grafted surface layer towards a specific polymer, which can be tuned by the choice of the grafted functional groups according to the specific structure of the polymer [28]. For example, the effect of nonpolar groups such as C18 chains on the bonding with non-polar polymers such as polyethylene will be investigated, while polar groups such as alkyl-amines will be used for the bonding of polymers such as polyether-ether-ketone or polyamide66.

4. Conclusions

The nanosecond laser patterning of titanium surface in ambient atmosphere followed by covalent grafting of alkyl groups through silanization and phosphonation reactions was performed in order to obtain dense and uniform aliphatic layers susceptible to enhance the chemical affinity of the titanium surface to nonpolar polymers. The main obtained conclusions are:

1. The light blue squama-like oxide layers composed by rutile and anatase were obtained on titanium surface by nanosecond laser treatment. The application of ultrasound cleaning allowed removing weakly-adhered rutile particles, but preserved the wavy oxide layer mostly composed by anatase. The matured samples showed hydrophobic behavior with static contact angle of 138° due to the accumulation of airborne organic impurities.
2. Amongst three tested silanization methods, the highest loading of modifier molecule (10 at.% Si) associated with formation of well-developed polycondensed siloxane layer was obtained by the functionalization of laser-treated surface in vapor phase of ODTMS. However, severe reaction conditions induced some damage to the superficial oxide layer. The silanization in pure liquid phase (DDTES) resulted in lower loading of the modifier (6 at.% Si), however, the oxide layers were undamaged. Finally, the modification in boiling THF solution of ODTMS was inefficient due to the insufficient chemical affinity of alkoxysilanes to TiO_2.
3. The functionalization in boiling water solutions of OPA allowed attaining full monolayer coverage of the surface (7 at.% P) for concentrations of 50 mM or higher. The results of XPS and Raman analysis indicate the dominating bidentate bonding of OPA.
4. For both silanization and phosphonation, the uniform distribution of modifier on the laser-treated surface was observed. The measurements of static contact angle indicated the similar increase in hydrophobicity (~150°) for the samples with maximum organic loading.
5. The functionalization with phosphonic acid is preferable because it can be performed with lower concentrations and temperatures compared to alkoxysilanes.
6. Future work will aim to optimize the combined effect of laser-induced surface patterning and chemical functionalization to develop effective inorganic-organic interfaces when joining or coating titanium alloys with polymers.

7. CRediT authorship contribution statement

Iryna Tomashchuk: Conceptualization, Investigation, Writing - Original Draft, Writing - Review & Editing, Visualization, Supervision, Project administration, Funding acquisition. **Liudmyla Kostenko:** Methodology, Investigation . **Jean-Marie Jouvard:** Methodology, Investigation, Funding acquisition. **Luc Lavisse:** Investigation, Writing - Review & Editing. **María del Carmen Marco de Lucas:** Investigation, Writing - Review & Editing.

8. Acknowledgements

This work was funded by BQR-2019 Interfaçage Hybride provided by the Scientific Committee of Laboratoire Interdisciplinaire Carnot de Bourgogne, UMR 6303 CNRS, by the Regional Council of Bourgogne Franche-Comté, the Graduate School EIPHI (Contract ANR-17-EURE-0002) and the FEDER.

Authors are thankful to Dr. Anna Sobolewska and Dr. Olivier Heintz (department Technique Analyses Instrumentation, Laboratoire Interdisciplinaire Carnot de Bourgogne, UMR 6303 CNRS, Université de Bourgogne Franche-Comté) for carrying out XPS analysis and their help in data processing and interpretation.

9. References

[1] D. Meroni, L. Presti,G. Di Liberto, M. Ceotto, R.G. Acres, K.C.Prince, R. Bellani, G. Soliveri, S. Ardizzone, A Close Look at the Structure of the TiO2-APTES Interface in Hybrid Nanomaterials and Its Degradation Pathway: An Experimental and Theoretical Study, J. Phys. Chem. C 121 (2017) 430–440. https://doi.org/10.1021/acs.jpcc.6b10720

[2] R. Helmy, A.Y. Fadeev, Self-Assembled Monolayers Supported on TiO_2: Comparison of $C_{18}H_{37}SiX_3$ (X = H, Cl, OCH_3), $C_{18}H_{37}Si(CH_3)_2Cl$, and $C_{18}H_{37}PO(OH)_2$, Langmuir 18, 23 (2002) 8924–8928. https://doi.org/10.1021/la0262506

[3] G. Guerrero, P. H. Mutin, and A. Vioux, Anchoring of Phosphonate and Phosphinate Coupling Molecules on Titania Particles, Chem. Mater.13 (2001) 4367–4373. https://doi.org/10.1021/cm001253u

[4] M.P. Danahy, M. J. Avaltroni, K. S. Midwood, J. E. Schwarzbauer, J. Schwartz, Self-assembled Monolayers of α,ω-Diphosphonic Acids on Ti Enable Complete or Spatially Controlled Surface Derivatization, Langmuir 20 (2004) 5333–5337. https://doi.org/10.1021/la036084h

[5] N. Adden, L. J. Gamble, D. G. Castner, A. Hoffmann, G. Gross, H. Menzel, Phosphonic Acid Monolayers for Binding of Bioactive Molecules to Titanium Surfaces, Langmuir 22 (2006) 8197–8204. https://doi.org/10.1021/la060754c

[6] C. Viornery, Y. Chevolot, D. Léonard, B.-O. Aronsson, P. Péchy, H. J. Mathieu, P. Descouts, M. Grätzel, Surface Modification of Titanium with Phosphonic Acid To Improve Bone Bonding: Characterization by XPS and ToF-SIMS, Langmuir 18 (2002) 2582–2589. https://doi.org/10.1021/la010908i

[7] J. Vaithilingam, S. Kilsby, R.D. Goodridge, S. D.R. Christie, S. Edmondson, R. J.M. Hague, Immobilisation of an antibacterial drug to Ti6Al4V components fabricated using selective laser melting, Appl. Surf. Sci. 314 (2014) 642-654. https://doi.org/10.1016/j.apsusc.2014.06.014

[8] J. Vaithilingam, S. Kilsby, R.D. Goodridge, S. D.R. Christie, S. Edmondson, R.J.M. Hague, Functionalisation of Ti6Al4V components fabricated using selective laser melting with a bioactive compound, Mater. Sci. Eng. C 46 (2015) 52-61. https://doi.org/10.1016/j.msec.2014.10.015

[9] M.C. Marco de Lucas, L. Lavisse, G. Pillon, Microstructural and tribilogical study of Nd :YAG laser treated titanium plates, Tribol. Internat. 41 (2008) 985-991. https://doi.org/10.1016/j.triboint.2008.03.007

[10] H. He, R. Hua, X. Li, C. Wang X. Ning, L. Sun, Fabrication of Superhydrophobic Ti-Al6-4V Surfaces with Single-Scale Microtextures by using Two-Step Laser Irradiation and Silanization, Materials 13 (2020), 3816. https://doi.org/10.3390/ma13173816

[11] C. Guo, M. Zhang, J. Hu, Fabrication of hierarchical structures on titanium alloy surfaces by nanosecond laser for wettability modification, Opt. Las. Technol. 148 (2022) 107728. https://doi.org/10.1016/j.optlastec.2021.107728

[12] D. Huerta-Murillo, A. Garcìa-Girón, J. M. Romano, J.T. Cardoso, F. Cordovilla, M. Walker, S.S. Dimov, J. L. Ocąña, Wettability modification of laser-fabricated hierarchical surface structures on Ti-6Al-4V titanium alloy, Appl. Surf. Sci. 463 (2019) 838-846. https://doi.org/10.1016/j.apsusc.2018.09.012

[13] L. Lavisse, J.M. Jouvard, L. Imhoff, O. Heintz, J. Korntheuer, C. Langlade, S. Bourgeois, M.C. Marco de Lucas, Pulsed laser growth and characterization of thin films on titanium substrates, Appl. Surf. Sci. 253 (2007) 8226-8230. https://doi.org/10.1016/j.apsusc.2007.02.136

[14] I. Shupyk, L. Lavisse, J.-M. Jouvard, M.C. Marco de Lucas, S. Bourgeois, F. Herbst, J.-Y. Piquemal, F. Bozon-Verduraz, M. Pilloz, Study of surface layers and ejected powder formed by oxidation of titanium substrates with a pulsed Nd:YAG laser beam, Appl. Surf. Sci. 255 (2009) 5574-5578. https://doi.org/10.1016/j.apsusc.2008.08.108

[15] V. Optasanu, E. Bourillot, R. Selon, L. Lavisse, A. Sanchot, P. Vitry, A. Kanjer, P. Berger, E. Lesniewska, T. Montesin, Characterization of Oxygen-Enriched Layers of TA6V, Titanium, and Zirconium by Scanning Microwave Microscopy, Oxid. Metals 88 (2016) 531-542. https://doi.org/10.1007/s11085-016-9678-0

[16] C. Demian, S. Costil, P. Sallamand, A. Soveja, H. Liao, S. Mattei, Laser densification of organic coating : Effects of laser wavelength, operating parameters and substrate properties, Surf. Coat. Technol. 206 (2012) 3526-3533. https://doi.org/10.1016/j.surfcoat.2012.02.032

[17] Y. Huang, X. Gao, Y. Zhang, B. Ma, Laser joining technology of polymer-metal hybrid structures – A review, J. Manuf. Process. 79 (2022) 934-961. https://doi.org/10.1016/j.jmapro.2022.05.026

[18] D.P. Adams, R.D. Murphy, D.J. Saiz, D.A. Hirschfeld, M.A. Rodriguez, P.G. Kotula, B.H. Jared, Nanosecond pulsed laser irradiation of titanium: Oxide growth and effects on underlying metal, Surf. Coat. Technol. 248 (2014) 38-45. https://doi.org/10.1016/j.surfcoat.2013.12.052

[19] A. J. Antończak, Ł. Skowroński, M. Trzcinski, V. V. Kinzhybalo, Ł. K. Łazarek, K. M. Abramski, Laser-induced oxidation of titanium substrate: Analysis of the physicochemical structure of the surface

and sub-surface layers, Appl. Surf. Sci. 325 (2015) 217-226. https://doi.org/10.1016/j.apsusc.2014.11.062

[20] P. Hubert Mutin, G. Guerrero, A. Vioux, Hybrid materials from organophosphorus coupling molecules, J. Mater. Chem. 15 (2005) 3761-3768. https://doi.org/10.1039/B505422B

[21] G. A. Sewvandi, Z. Tao, T. Kusunose, Y. Tanaka, S. Nakanishi, Q. Feng, Modification of TiO_2 Electrode with Organic Silane Interposed Layer for High-Performance of Dye-Sensitized Solar Cells, ACS Appl. Mater. Interfaces 6 (2014) 5818–5826. https://doi.org/10.1021/am500666e

[22] M. Psarski, G. Celichowski, E. Bystrzycka, D. Pawlak, J. Grobelny, M. Cichomski, Vapor phase deposition of fluoroalkyl trichlorosilanes on silicon and glass: Influence of deposition conditions and chain length on wettability and adhesion forces, Mater. Chem. Phys. 204 (2018) 305-314. https://doi.org/10.1016/j.matchemphys.2017.10.037

[23] T. Sultana, G.L. Georgiev, G. Auner, G. Newaz, H. J. Herfurth, R. Patwa, XPS analysis of laser transmission micro-joint between poly (vinylidene fluoride) and titanium, Appl. Surf. Sci. 255 (2008), 2569-2573. https://doi.org/10.1016/j.apsusc.2008.07.149

[24] G. L. Georgiev, R. J. Baird, E. F. McCullen, G. Newaz, G. Auner, R. Patwa, H. Herfurth, Chemical bond formation during laser bonding of Teflon® FEP and titanium, Appl. Surf. Sci. 255:15 (2009) 7078-7083. https://doi.org/10.1016/j.apsusc.2009.03.046

[25] S. Bhowmik, R. Benedictus, J.A. Poulis, H. W. Bonin, V. T. Bui, High-performance nanoadhesive bonding of titanium for aerospace and space applications, Internat J. Adhes. Adhes. 29 (2009) 259-267. https://doi.org/10.1016/j.ijadhadh.2008.07.002

[26] J. Moritz, P. Götze, T. Schiefer, L. Stepien, A. Klotzbach, J. Standfuß E. López, F. Brückner, C. Leyens, Additive Manufacturing of Titanium with Different Surface Structures for Adhesive Bonding and Thermal Direct Joining with Fiber-Reinforced Polyether-Ether-Ketone (PEEK) for Lightweight Design Applications, Metals 11:2(2021). 265. https://doi.org/10.3390/met11020265

[27] K. Kondoh, J. Umeda, CO bond enhancing direct bonding strength between plastic and pure titanium, Mat. Lett. 211 (2018) 331-334. https://doi.org/10.1016/j.matlet.2017.10.042

[28] C. Tan, J. Su, Y. Liu, Z. Feng, X. Song, X. Wang, B. Chen, H. Xia, Enhanced interfacial bonding strength of laser bonded titanium alloy/CFRTP joint via hydrogen bonds interaction, Comp. Part B: Engineer. 239 (2022) 109966. https://doi.org/10.1016/j.compositesb.2022.109966

[29] F. Torrent, L. Lavisse, P. Berger, J.-M. Jouvard, H. Andrzejewski, G. Pillon, S. Bourgeois, M.C. Marco de Lucas, Wavelength influence on nitrogen insertion into titanium by nanosecond pulsed laser irradiation in air, Appl. Surf. Sci. 278 (2013) 245-249. https://doi.org/10.1016/j.apsusc.2012.11.110

[30] La Surface.com http://lasurface.com/database/elementxps.php (accessed 6 April 2022).

[31] H. Okamoto, O-Ti (Oxygen-Titanium). J. Phase Equilib. Diffus. 32 (2011) 473-474. https://doi.org/10.1007/s11669-011-9935-5

[32] J. L. Murray, H. A. Wriedt, The O-Ti (oxygen-titanium) system, Bull. Alloy Phase Diagrams 8 (1987) 148–165. https://doi.org/10.1007/BF02873201

[33] T. Ohsaka, F. Izumi, Y. Fujiki, Raman spectrum of anatase TiO_2, J. Raman Spectr. 7 (1978) 321-324. https://doi.org/10.1002/jrs.1250070606

[34] S.P.S. Porto, P.A. Fleury, T.C. Damen, Raman spectra of TiO_2, MgF_2, ZnF_2, FeF_2 and MnF_2, Phys. Review 154 (1967) 522-526. https://doi.org/10.1103/PhysRev.154.522

[35] D.A.H. Hanaor, C.C. Sorrell, Review of the anatase to rutile phase transformation, J. Mater. Sci. 46 (2011) 855–874. https://doi.org/10.1007/s10853-010-5113-0

[36] D. Kuczyńska-Zemła, G. Sundell, M. Zemła, M. Andersson, H. Garbacz, The distribution of O and N in the surface region of laser-patterned titanium revealed by atom probe tomography, Appl. Surf. Sci. 562 (2021) 150193. https://doi.org/10.1016/j.apsusc.2021.150193

[37] R. Castaing, Electron Probe Microanalysis, Adv. Electronics and Electron Phys. 13 (1960) 317-386. https://doi.org/10.1016/S0065-2539(08)60212-7

[38] C.-J. Yang, X.-S. Mei, Y.-L. Tian, D.-W. Zhang, Y. Li, X. Liu, Modification of wettability property of titanium by laser texturing, Int. J. Adv. Manuf. Technol. 87 (2016) 1663–1670. https://doi.org/10.1007/s00170-016-8601-9

[39] J. Lu, T. Huang, Z. Liu, X. Zhang, R. Xiao, Long-term wettability of titanium surfaces by combined femtosecond micro/nano structuring and chemical treatments, Appl. Surf. Sci. 459 (2018) 257-262. https://doi.org/10.1016/j.apsusc.2018.08.004

[40] H.-Q. Dou, H. Liu, S. Xu, Y. Chen, X. Miao, H. Lü, X. Jiang, Influence of laser fluences and scan speeds on the morphologies and wetting properties of titanium alloy, Optik 244 (2020) 165443. https://doi.org/10.1016/j.ijleo.2020.165443

[41] D. H. Do, C. Walgraeve, A. N. Amare, K. R. Barai, A. Estigoy Parao, K. Demeestere, H. van Langenhove, Airborne volatile organic compounds in urban and industrial locations in four developing countries, Atm. Environment 119 (2015) 330-338. https://doi.org/10.1016/j.atmosenv.2015.08.065

[42] D. H. Do, H. van Langenhove, C. Walgraeve, S. F. Hayleeyesus, P. de Wispelaere, J. Dewulf, K. Demeestere, Volatile organic compounds in an urban environment: a comparison among Belgium, Vietnam and Ethiopia, Internat. J. Environ. Anal. Chem. 93:3 (2013) 298-314. https://doi.org/10.1080/03067319.2011.620708

[43] M. F. Mohamed, D. Kang, V. P. Aneja, Volatile organic compounds in some urban locations in United States, Chemosphere 47 (2002) 863-882. https://doi.org/10.1016/S0045-6535(02)00107-8

[44] A. Baudic, V. Gros, S. Sauvage, N. Locoge, O. Sanchez, R. Sarda-Estève, C. Kalogridis, J.-E. Petit, N. Bonnaire, D. Baisnée, O. Favez, A. Albinet, J. Sciare, B. Bonsang, Seasonal variability and source apportionment of volatile organic compounds (VOCs) in the Paris megacity (France), Atmos. Chem. Phys. 16 (2016) 11961–11989. https://doi.org/10.5194/acp-16-11961-2016

[45] S.C. Lee, M.Y. Chiu, K.F. Ho, S.C. Zou, X. Wang, Volatile organic compounds (VOCs) in urban atmosphere of Hong Kong, Chemosphere 48:3 (2002) 375-382. https://doi.org/10.1016/S0045-6535(02)00040-1

[46] R. N. Wenzel, Resistance of solid surfaces to wetting by water, Ind. Eng. Chem. 28 (1936) 988-994. https://doi.org/10.1021/ie50320a024

[47] R. Helmy, A. Y. Fadeev, Self-Assembled Monolayers Supported on TiO2: Comparison of C18H37SiX3 (X = H, Cl, OCH3), C18H37Si(CH3)2Cl, and C18H37PO(OH)2, Langmuir 18 (2002) 8924–8928. https://doi.org/10.1021/la0262506

[48] M.E Simonsen, C. Sønderby, Z. Li, E.G. Søgaard, XPS and FT-IR investigation of silicate polymers, J. Mater. Sci. 44 (2009) 2079–2088. https://doi.org/10.1007/s10853-009-3270-9

[49] F. Torrent, Functionalization of metallic surfaces by titanium oxynitrides thin films obtained by laser irradiation under controlled atmosphere and by PVD, PhD thesis, Université de Bourgogne, 2013. http://www.theses.fr/2013DIJOS053

[50] P. Kofstad, High-temperature oxidation of titanium, J. Less Common Metals 12:6 (1967) 449-464. https://doi.org/10.1016/0022-5088(67)90017-3

[51] A. Baptiste, A. Gibaud, J. F. Bardeau, X-ray, Micro-Raman, and Infrared Spectroscopy Structural Characterization of Self-Assembled Multilayer Silane Films with Variable Numbers of Stacked Layers, Langmuir 18 (2002) 3916-3922. https://doi.org/10.1021/la015572r

[52] D.M. Spori, N. V. Venkataraman, S.G.P. Tosatti, F. Durmaz, N.D. Spencer, S. Zürcher, Influence of Alkyl Chain Length on Phosphate Self-Assembled Monolayers, Langmuir 23 (2007) 8053–8060. https://doi.org/10.1021/la700474v

[53] M. Textor, L. Ruiz, R. Hofer, A. Rossi, K. Feldman, G. Hähner, N. D. Spencer, Structural Chemistry of Self-Assembled Monolayers of Octadecylphosphoric Acid on Tantalum Oxide Surfaces, Langmuir 16 (2000) 3257-3271. https://doi.org/10.1021/la990941t

[54] P.A. Orrillo, S.B. Ribotta, L.M. Gassa, G. Benítez, R.C. Salvarezza, M.E. Vela, Phosphonic acid functionalization of nanostructured Ni–W coatings on steel, Appl. Surf. Sci. 433 (2018) 292-299. https://doi.org/10.1016/j.apsusc.2017.09.222

[55] B. Adolphi, E. Jähne, G. Busch, X. Cai, Characterization of the adsorption of omega-(thiophene-3-yl alkyl) phosphonic acid on metal oxides with AR-XPS, Anal. Bioanal. Chem. 379(2004) 646-52. https://doi.org/10.1007/s00216-004-2634-x

[56]N. Metoki, L. Liu, E. Beilis, N. Eliaz, D. Mandler, Preparation and Characterization of Alkylphosphonic Acid Self-Assembled Monolayers on Titanium Alloy by Chemisorption and Electrochemical Deposition, Langmuir 30 (2014) 6791–6799. https://doi.org/10.1021/la404829b

[57] G. Zorn, I. Gotman, E. Y. Gutmanas, R. Adadi, C. N. Sukenik, Surface modification of Ti45Nb alloy by immobilization of RGD peptide via self assembled monolayer, J. Mater. Sci. Mater. Med. 18 (2007) 1309-15. https://doi.org/10.1007/s10856-006-0117-7

[58]S. Tosatti, R. Michel, M. Textor, N. D. Spencer, Self-Assembled Monolayer of Dodecyl and Hydroxy-Dodecyl Phosphate at Smooth and Rough Titanium and Titanium Oxide Surfaces, Langmuir 18 (2002) 3537-3548. http://dx.doi.org/10.1021/La011459p

[59] R. Hofer, M. Textor, and N. D. Spencer, Alkyl Phosphate Monolayers, Self-Assembled from Aqueous Solution onto Metal Oxide Surfaces, Langmuir 17 (2001) 4014–4020. https://doi.org/10.1021/la001756e

[60] S. M. Kuznetsov, V. S. Novikov, E. A. Sagitova, L. Yu. Ustynyuk, A. A. Glikin, K. A. Prokhorov, G. Yu. Nikolaeva, P. P. Pashinin, Raman spectra of n-pentane, n-hexane, and n-octadecane: experimental and density functional theory (DFT) study, Laser Phys. 29 (2019) 085701. https://doi.org/10.1088/1555-6611/ab2908

[61] A.Vega, P. Thissen, Y. J. Chabal, Environment-Controlled Tethering by Aggregation and Growth of Phosphonic Acid Monolayers on Silicon Oxide, Langmuir 28 (2012) 8046–8051. https://doi.org/10.1021/la300709n

[62] P. J. Hotchkiss, M. Malicki, A. J. Giordano, N.R. Armstrong, S.R. Marder, Characterization of phosphonic acid binding to zinc oxide, J. Mater. Chem. 21 (2011) 3107–3112. https://doi.org/10.1039/C0JM02829K

[63] S. Attavar, M.Diwekar, M. R. Linford, M. A. Davis, S.Blair, Passivation of aluminum with alkyl phosphonic acids for biochip applications, Appl. Surf. Sci. 256 (2010) 7146-7150. https://doi.org/10.1016/j.apsusc.2010.05.041

[64] M. Cichomski, K. Kośla, J. Grobelny, W. Kozłowski, W. Szmaja, Tribological and stability investigations of alkylphosphonic acids on alumina surface, Appl. Surf. Sci. 273 (2013) :570-577, https://doi.org/10.1016/j.apsusc.2013.02.081

[65] M. A. Frank, C. Meltzer, B. Braunschweig, W. Peukert, A. R. Boccaccini, S. Virtanen, Functionalization of steel surfaces with organic acids: Influence on wetting and corrosion behavior, Appl. Surf. Sci. 404 (2017) 326-333. https://doi.org/10.1016/j.apsusc.2017.01.199

[66] R. Bhure, T. M. Abdel-Fattah, C. Bonner, F. Hall, A. Mahapatro, Stability of Phosphonic Self Assembled Monolayers (SAMs) on Cobalt Chromium (Co-Cr) Alloy under Oxidative conditions. Appl. Surf. Sci. 257(2011):5605-5612. doi:10.1016/j.apsusc.2011.01.055

[67] G. Zorn, I. Gotman, E. Y. Gutmanas, R. Adadi, G. Salitra, and C. N. Sukenik, Surface Modification of Ti45Nb Alloy with an Alkylphosphonic Acid Self-Assembled Monolayer, Chem. Mater. 17 (2005) 4218–4226. https://doi.org/10.1021/cm050477f

[68]A. Kanta, R. Sedev, J. Ralston, The formation and stability of self-assembled monolayers of octadecylphosphonic acid on titania, Coll. Surf. A: Physicochem. Eng. Aspects 291 (2006) 51-58. https://doi.org/10.1016/j.colsurfa.2005.12.057

Covalent grafting of alkyl chains on laser-treated titanium surfaces through silanization and phosphonation reactions

Supplementary information

Iryna TOMASHCHUK[a*], Liudmyla KOSTENKO[b], Jean-Marie JOUVARD[a], Luc LAVISSE[c], María del Carmen MARCO de LUCAS[c]

[a] Laboratoire Interdisciplinaire Carnot de Bourgogne, UMR 6303 CNRS, Université Bourgogne Franche-Comté, 12 rue de la Fonderie, 71200 Le Creusot, France. E-mails: iryna.tomashchuk@u-bourgogne.fr; jean-marie.jouvard@u-bourgogne.fr.
[b] Faculty of Chemistry, Taras Shevchenko National University of Kyiv, Lva Tolstoho Street 12, 01033 Kyiv, Ukraine; E-mail: lskostenko69@gmail.com .
[c] Laboratoire Interdisciplinaire Carnot de Bourgogne, UMR 6303 CNRS, Université Bourgogne-Franche Comté, 9 Avenue A. Savary, BP 47 870, F-21078 Dijon Cedex, France. E-mails: luc.lavisse@u-bourgogne.fr; delucas@u-bourgogne.fr.
*corresponding author

Additional characterization of laser-treated surface before US cleaning

XRD analysis of the laser-treated surface was made with PANalytical X'Pert PRO, using a Co target, with a scan step of 0.017°, a scanning range of 20-120° and a counting time of 600 s per step. XRD analysis of the laser-treated substrate showed the peaks of stoichiometric oxides TiO_2, both rutile and anatase along with Ti_2O_3 and sub-stoichiometric oxide Ti_3O (Figure A). A high peak of native α-Ti indicates that the penetration of X-rays was superior to the total depth of oxide layer and the diffraction occurred in all oxide phases existing in the sample. The light-blue color of such surfaces and the presence of TiO_2 and Ti_2O_3 phases were previously described by Antończak et al. [a] as the most oxidized substrates obtainable by nanosecond laser processing.

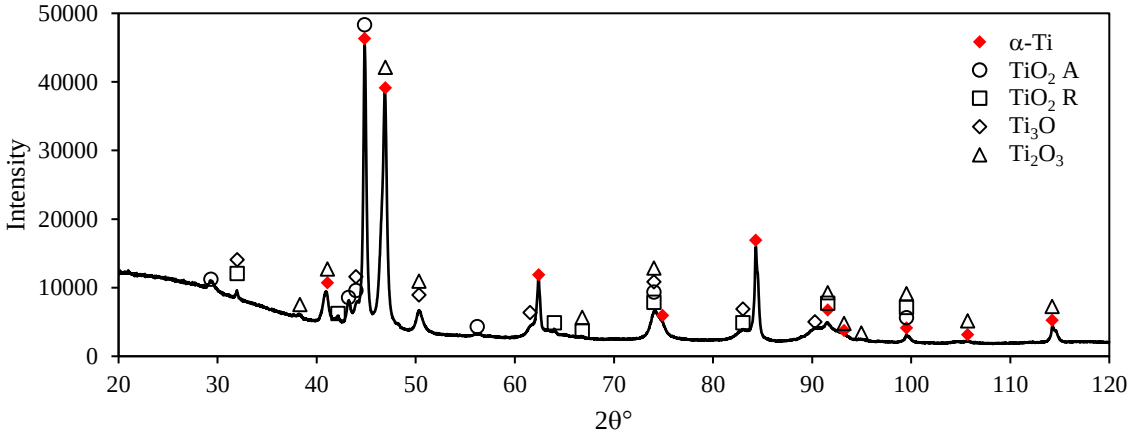

Figure A. XRD spectrum of laser-treated substrate before US cleaning.

Raman analysis of the surface before US cleaning (Figure B) indicated that the numerous white particles were mostly composed by rutile. On the rest of the surface, anatase was the dominating oxide, with some addition of rutile. The ultrasound cleaning of the sample induced the massive loss of weakly adhered rutile-based particles.

[a]A. J. Antończak, Ł. Skowroński, M. Trzcinski, V. V. Kinzhybalo, Ł. K. Łazarek, K. M. Abramski, Laser-induced oxidation of titanium substrate: Analysis of the physicochemical structure of the surface and sub-surface layers, Appl. Surf. Sci. 325 (2015) 217-226. https://doi.org/10.1016/j.apsusc.2014.11.062

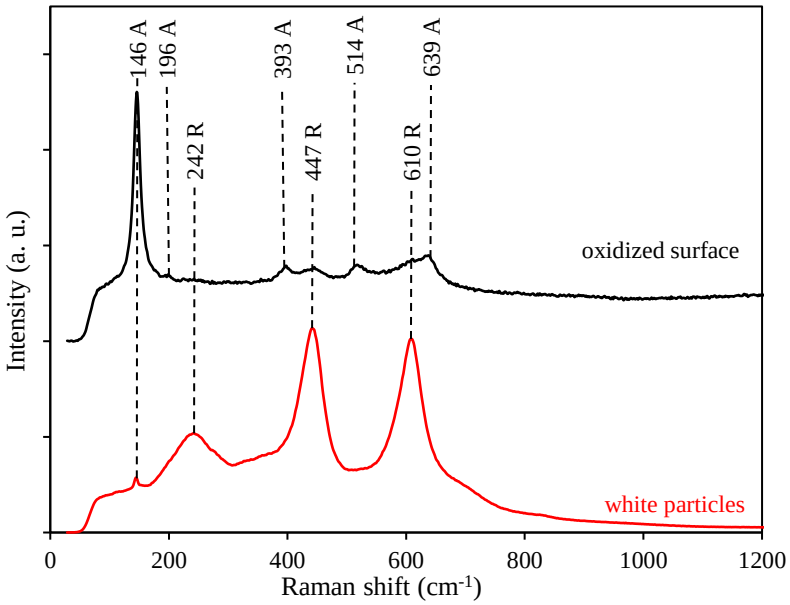

Figure B. Raman analysis of the laser-treated surface before US cleaning.

Imaging of contact angles measurements in chemically functionalized samples

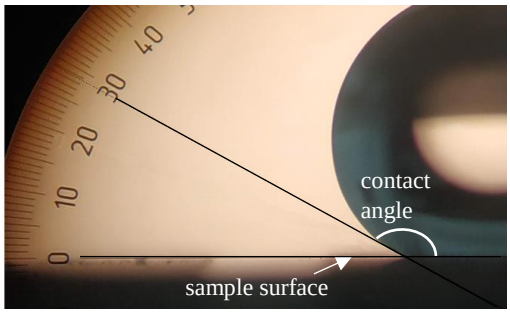

Figure C. Static contact angle on the surface of Si-D.

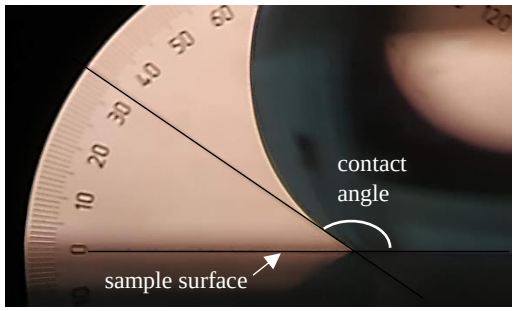

Figure D. Static contact angle on the surface of P5.6.

Assignment of vibrational frequencies of free and bonded phosphonic acid

Table A. Literature data on vibrational frequencies (cm^{-1}) of free and bonded phosphonic groups.

Products	**Method**	**Bonding**	***v*(P-OH)**	***v*(P-O)**	***v*(P=O)**	***v*(C-P)**	**δ(C-P)**	**δ(O-P-OH)**	**γ(O-P-OH)**	**Ref.**
ODPA	FTIR	Unbonded	955, 1000	-	1230	-	-	-	-	[b]
ODPA-ITO	PM-IRRAS	Mono + bidentate	933		1230					
ODPA-ZnO	IRRAS	Tridentate	-	1016 with shoulder	-	-	-	-	-	[c]
ODPA	FTIR	Unbonded	955,930,1000	-	1230	-	-	-	-	[d]
ODPA-ITO	PM-IRRAS	Mono +bidentate	933	970-1124 as.,1000-1070 s.	1230					
ODPA	FTIR	Unbonded	956	-	1227	-	-	-	-	[e]
ODPA-SiO_2	FTIR	Bidentate	-	1108, 1080 (shoulder)	1227					
ODPA	FTIR	Unbonded	957, 948, 932	1077, 1003	1225, 1215	-	-	-	-	[f]
ODPA-ZnO	FTIR	Bi- or tridentate	-	1116,1050,980,951	1170					
ODPA	ATR-IR	Unbonded	957, 948, 933	1076, 1005	1227, 1217	-	-	-	-	[g]
ODPA-nitinol	ATR-IR	Monodent.	957, 948, 932	1060, 1005	1227, 1217					
ODPA	Raman	Unbonded	950	1000-1150	-	-	-	-	-	[h]
ODPA-NiW	Raman	Not discussed	-	1000-1150	-					
PPA	Calc. DFT	Unbonded	870 as., 821 s.	-	1264	1123	-	-		[i]
PPA-TiO_2(A)	Calc. DFT	Monodent.	1046 as., 934 s.	1061	-	1124				
	Calc. DFT	Bidentate	-	1033, 1001, 945, 928, 902	1101	1117, 1136				
	Calc. DFT	Tridentate	-	971, 955, 915	-	1100				
2-oxo-2(thiophen-2-yl)ethyl PA	Raman	Unbonded	797, 848	-	1297	710	174, 177	471, 456, 428, 422	252	[j]
(hydroxypyridin-3-yl-methyl) PA	FT-Raman	Unbonded -PO_3H_2	-	1040, 1012	1225	-	-	-	-	[k]
	FTIR	Unbonded -PO_3H^-	-	1054, 1034	1272					
		Unbonded -PO_3^{2-}	-	1053, 875	1168					

[b] P. J. Hotchkiss, S.C. Jones, S.A. Paniagua, A. Sharma, B. Kippelen, N.R. Armstrong, S.R. Marder, The Modification of Indium Tin Oxide with Phosphonic Acids: Mechanism of Binding, Tuning of Surface Properties, and Potential for Use in Organic Electronic Applications, Acc. Chem. Res.45 (2012) 337–346. https://doi.org/10.1021/ar200119g

[c] P. J. Hotchkiss, M. Malicki, A. J. Giordano, N.R. Armstrong, S.R. Marder, Characterization of phosphonic acid binding to zinc oxide, J. Mater. Chem 21 (2011) 3107–3112. https://doi.org/10.1039/C0JM02829K

[d] S. A. Paniagua, P. J. Hotchkiss, S. C. Jones, S.R. Marder, A. Mudalige, F. S. Marrikar, J. E. Pemberton, N. R. Armstrong, Phosphonic Acid Modification of Indium−Tin Oxide Electrodes: Combined XPS/UPS/Contact Angle Studies, J. Phys. Chem. C 112 (2008) 7809–7817. https://doi-org.inp.bib.cnrs.fr/10.1021/jp710893k

[e] A.Vega, P. Thissen, Y. J. Chabal, Environment-Controlled Tethering by Aggregation and Growth of Phosphonic Acid Monolayers on Silicon Oxide, Langmuir 28 (2012) 8046–8051. https://doi.org/10.1021/la300709n

[f] R. Quiñones, K. Rodriguez, R. J. Iuliucci, Investigation of phosphonic acid surface modifications on zinc oxide nanoparticles under ambient conditions, Thin Solid Films 565 (2014) 155-164. https://doi.org/10.1016/j.tsf.2014.06.057

[g] R. Quiñones, S. Garretson, G. Behnke, J. W. Fagan, K. T. Mueller, S.Agarwal, R. K. Gupta, Fabrication of phosphonic acid films on nitinol nanoparticles by dynamic covalent assembly, Thin Solid Films 642 (2017) 195-206. https://doi.org/10.1016/j.tsf.2017.09.048

[h] P.A. Orrillo, S.B. Ribotta, L.M. Gassa, G. Benítez, R.C. Salvarezza, M.E. Vela, Phosphonic acid functionalization of nanostructured Ni–W coatings on steel, Appl. Surf. Sci. 433 (2018) 292-299. https://doi.org/10.1016/j.apsusc.2017.09.222

[i] D. Geldof, M. Tassi, R. Carleer, P. Adriaensens, A. Roevens, V. Meynen, F. Blockhuys, Binding modes of phosphonic acid derivatives adsorbed on TiO2 surfaces: Assignments of experimental IR and NMR spectra based on DFT/PBC calculations, Surf. Sci. 655 (2017) 31-38. https://doi.org/10.1016/j.susc.2016.09.001

[j] H. Lamsaf, M. I. L. Soares, S. M.V. Pinto, E. M. Brás, M. S.C. Henriques, J. A. Paixão, A. Oulmekki, E. H. Elghadraoui, R. Fausto, Molecular and crystal structures and spectroscopic properties of 2-oxo-2-(Thiophen-2-yl) ethyl phosphonic acid, J. Mol. Struct. 1178 (2019) 73-82. https://doi.org/10.1016/j.molstruc.2018.10.015

[k] M. Baranska, A. Wesełucha-Birczynska, K. Chruszcz-Lipska, L. M. Proniewicz, FT-Raman study of (hydroxypyridin-3-yl-methyl)phosphonic acid with varying pH: 2D correlation method, Vibrat. Spectroscopy 35 (2004) 233-237. https://doi.org/10.1016/j.vibspec.2004.02.006